# A WENO FINITE-DIFFERENCE SCHEME FOR A NEW CLASS OF HAMILTON-JACOBI EQUATIONS IN ELECTROELASTOSTATICS

BY

ALVARO DAVID GARNICA

THESIS

Submitted in partial fulfillment of the requirements
for the degree of Master of Science in Civil Engineering
in the Graduate College of the
University of Illinois at Urbana-Champaign, 2016

Urbana, Illinois

Adviser:

Professor Oscar Lopez-Pamies

# ABSTRACT

Hamilton-Jacobi equations have repeatedly emerged in many fields of physics, most notably, optimal control, differential games, geometric optics, and image processing. This thesis presents a new numerical method to solve a new class of Hamilton-Jacobi equation that has recently appeared in the context of nonlinear electroelastostatics.

In a pioneering contribution, Crandall and Lions (1983) proved that a certain type of first-order finite difference method converges to the viscosity solution of a special class of Hamilton-Jacobi equations. From then on several successful methods of high-order approximation have been proposed in the literature, including the so-called WENO finite difference schemes. These schemes, however, were developed and tested for special classes of Hamilton-Jacobi equations, which do not include the general type of Hamilton-Jacobi equation of interest in this work. The objective of this thesis is to extend high-order WENO finite difference schemes to the most general type of Hamilton-Jacobi equations involving non-periodic boundary conditions in the "space" variables.

Following its derivation, the proposed WENO scheme is tested for several cases involving one and two "space" variables for which there are analytical solutions available for arbitrarily large values of the "time" variable. These numerical experiments provide insight into the stability and rate of convergence of the method as "time" increases. They also provide insight into how errors propagate into the domain of computation due to non-periodic boundary conditions.

This thesis concludes with the application of the method to compute the effective stored-energy function of an elastomer containing an isotropic distribution of vacuous pores under arbitrary 3D deformations.

# Contents

# 1 Introduction

By means of a combination of iterative techniques Lopez-Pamies (2014) has recently put forward an exact solution for the homogenized (or macroscopic) coupled electromechanical response of a general class of two-phase elastic particulate microstructures under finite deformations and finite electric fields. The result is given in terms of an effective free energy function which is defined implicitly as the solution of a Hamilton-Jacobi partial differential equation (pde). Denoting $\mathbf{F}$ and $\mathbf{E}$ the macroscopic deformation gradient and Lagrangian electric fields, by $W^{(1)}$ and $W^{(2)}$ the free energy functions describing the elastic dielectric response of the underlying matrix and particles and by $p_0^{(2)} = c$ and $p_0^{(22)}$ the one-and two-point correlation functions describing the spatial distribution of particles, the Hamilton-Jacobi pde for the effective free energy function $W = W(\mathbf{F}, \mathbf{E}, c)$ reads as

$$\frac{\partial W}{\partial c} + H\left(\mathbf{F}, \mathbf{E}, c, W, \frac{\partial W}{\partial \mathbf{F}}, \frac{\partial W}{\partial \mathbf{E}}\right) = 0; \qquad W(\mathbf{F}, \mathbf{E}, 1) = W^{(2)}(\mathbf{F}, \mathbf{E}) \tag{1}$$

with Hamiltonian

$$H = -\frac{W}{c} - \frac{1}{c}\int_{|\boldsymbol{\xi}|=1} \max_{\boldsymbol{\alpha}} \min_{\beta} \left[\boldsymbol{\alpha} \cdot \frac{\partial W}{\partial \mathbf{F}}\boldsymbol{\xi} + \beta \frac{\partial W}{\partial \mathbf{E}}\boldsymbol{\xi} - W^{(1)}(\mathbf{F} + \boldsymbol{\alpha} \otimes \boldsymbol{\xi}, \mathbf{E} + \beta\boldsymbol{\xi})\right] \nu(\boldsymbol{\xi}) d\boldsymbol{\xi} \tag{2}$$

where $\mathbf{F} \in M_+^{n\times n}$, $\mathbf{E} \in \mathbb{R}$, $c \in [0,1]$, and for particles that are randomly distributed

$$\nu(\boldsymbol{\xi}) = -\frac{1}{8\pi^2}\int_{\Omega_0} \frac{p_0^{(22)} - c^2}{(1-c)c} \delta''(\boldsymbol{\xi} \cdot \mathbf{X}) d\mathbf{X} \tag{3}$$

In this last expression $\Omega_0$ stands for the domain occupied by the material in its undeformed configuration and $\delta$" denotes the second derivative of the Dirac delta function. The constitutive response of the material is given by the free energy function $W$ simply by

$$\mathbf{S} = \frac{\partial W}{\partial \mathbf{F}}(\mathbf{F}, \mathbf{E}, c) \qquad \mathbf{D} = -\frac{\partial W}{\partial \mathbf{E}}(\mathbf{F}, \mathbf{E}, c) \tag{4}$$

where $\mathbf{S}$ and $\mathbf{D}$ stand for the macroscopic first Piola-Kirchoff stress and macroscopic Lagrangian electric displacement.

We refer to Lopez Pamies (2014) for the derivation and detailed description of the above result. Here it suffices to recall that the Hamilton-Jacobi equation (1) with (2), in addition to its theoretical value in providing rigorous solution for the electromechanical response of elastic dielectrics with a general class of particulate microstructure provides a formidable tool to investigate a wide range of fundamental phenomena from the bottom up and by the same token, to carry out material design. For example, in the absence of an electrical field when $E = 0$, the pde (1) with (2) has enabled the construction of a closed-form solution for the fundamental problem of the overall elastic response of Gaussian (Neo-Hookean) rubber weakened by a dilute distribution of vacuous

cavities, which in turn has led to the formulation of a new theory of cavitation and rubber (Lopez-Pamies et a1., 2011a; 2011b). It has also enabled the construction of a closed-form solution for the parallel fundamental problem of the overall elastic response of Gaussian rubber reinforced by a dilute isotropic distribution of rigid particles under arbitrarily large deformations (Lopez-Pamies et a1., 2013). In the presence of an electric field when $\mathbf{E} \neq 0$, more recently, the pde (1) with (2) has also been used to generate a closed-form solution for the overall electromechanical response for emerging dielectric elastomer composites in the "*clasical*" limit of small deformation and moderate electric fields (Spinelli et a1., 2015). The above-cited examples have allowed for analytical solutions of (1)-(2) partly because they correspond to limiting cases ($c \to 0+$ and $\mathbf{F} \to \mathbf{I}$, $\mathbf{E} \to \mathbf{0}$ ) amenable to tractable asymptotic analyses. In general, however equations (1)-(2) do not admit analytical solution. The objective of this paper is to provide a robust scheme to generate accurate numerical approximations for the viscosity solution (Crandall and Lions, 1983) of the general class of Hamilton-Jacobi equations (1) with (2), while possibly exhibiting steep gradients, is expected to be at least $C^2$, granted that the free energy functions $W^{(1)}$ and $W^{(2)}$ characterizing the elastic dielectric behaviors of the matrix and particles are smooth. This is in contrast to the viscosity solutions encountered in the majority of Hamilton-Jacobi equations that have been studied in the literature, which are Lipschitz continuous but not $C^1$ (see, e.g., Bardi and Capuzzo-Dolcetta 1997; Osher and Fedkiw, 2003; Toro, 2009). The expected (at least) $C^2$ character of the viscosity solution of (1) with (2) is believed to be due to the explicit dependence of the Hamiltonian on the function $W$ itself. If this regard, it is important to remark that the Hamiltonian (2) is in fact of general type as it depends explicilty as well on the "time" variable "$c$", on the "space" variables $\mathbf{F}$, $\mathbf{E}$, and on the gradients $\partial W/\partial \mathbf{F}$, $\partial W/\partial \mathbf{E}$.

## 2 Proposed scheme

The first part of this section, subsection 2.1. is dedicated to recording some general introductory remarks about WENO schemes, introducing some notation, and deriving the WENO approximations of the derivatives of a multivariable scalar-valued function required in the subsequent development. The "space" and "time" discretizations of the Hamilton-Jacobi equations (1) - (2) are undertaken in subsection 2.2. and 2.3. respectively.

### 2.1 WENO approximation of the partial derivatives of a multivariable scalar-valued function

WENO finite-differences schemes were originally introduced in 1996 by Jiang and Shu, as a generalization of the pioneering work of Liu, Osher, and Chan (1994) on WENO finite-volume schemes, within the context of hyperbolic conservation laws and have become increasingly popular over the last twenty years as a method of choice to solve numerically convection dominated pdes. The defining feature of WENO schemes is that they provide the means to reach arbitrarily high order accuracy (at least formally) in smooth regions of the solution while being able to describe in a non-oscillatory manner regions of discontinuous or steep gradients. For more details about WENO schemes, including an overview of their increasing application to an admittedly broad range of physical problems, we refer the interested reader to the excellent review of Shu (2009). For later use in the "space" discretization of the Hamilton-Jacobi equation (1)-(2), we derive below fifth-order WENO approximation formulas for the partial derivatives of multivariable scalar-valued functions.

#### 2.1.1 WENO approximation of the derivative of a single-variable function u(x)

We begin defining the WENO approximation of the derivative $u_x(x) = du(x)/dx$ of scalar-valued function $u(x)$ in terms of its points values $u_i = u(x_i)$ on a Cartesian grid $x_0 < x_1 < x_2 < ... < x_{m-1} < x_m$ with $x_{i+1} - x_i = h$ for all $i = \{0, 1, 2, ..., m\}$, where h is a constant.

The left-biased WENO approximation. Consider the four-point stencil $S_1^- = \{x_{i-3}, x_{i-2}, x_{i-1}, x_i\}$. It follows that there exists a unique polynomial $p_1^-(x)$ of degree three which interpolates the function $u(x)$ at the grid points in $S_1^-$. Further, the derivative $dp_1^-/dx$ of such a polynomial serves to approximate the derivative of the function $u_x(x)$ in $S_1^-$. In particular, assuming that the function u(x) is smooth in the stencil $S_1^-$, we have at $x = x_i$

$$u_x(x_i) = u_{x,i}^{-1} + O(h^3) \tag{5}$$

where

$$u_x^{-1}(x_i) = \frac{dp_1^-}{dx}(x_i) = \frac{1}{3}\frac{\Delta^+ u_{i-3}}{h} - \frac{7}{6}\frac{\Delta^+ u_{i-2}}{h} + \frac{11}{6}\frac{\Delta^+ u_{i-1}}{h} \tag{6}$$

Here and subsequently $\Delta^+ v_k = v_{k+1} - v_k$. Similarly considering the different stencil $S_2^- = \{x_{i-2}, x_{i-1}, x_i, x_{i+1}\}$, a different interpolating polynomial $p_2^-(x)$ would result such that, assuming that the function u(x) is smooth in $S_2^-$,

$$u_x(x_i) = u_{x,i}^{-2} + O(h^3) \tag{7}$$

where

$$u_x^{-2}(x_i) = \frac{dp_2^-}{dx}(x_i) = -\frac{1}{6}\frac{\Delta^+ u_{i-2}}{h} + \frac{5}{6}\frac{\Delta^+ u_{i-1}}{h} + \frac{1}{3}\frac{\Delta^+ u_i}{h} \tag{8}$$

By considering the stencil $S_3^- = \{x_{i-1}, x_i, x_{i+1}, x_{i+2}\}$, yet a different polynomial $p_3^-(x)$ would result such that, assuming that the function $u(x)$ is smooth in $S_3^-$,

$$u_x(x_i) = u_{x,i}^{-3} + O(h^3) \tag{9}$$

$$u_x^{-3}(x_i) = \frac{dp_3^-}{dx}(x_i) = \frac{1}{3}\frac{\Delta^+ u_{i-1}}{h} + \frac{5}{6}\frac{\Delta^+ u_i}{h} - \frac{1}{6}\frac{\Delta^+ u_{i-1}}{h} \tag{10}$$

Having generated approximations (6), (8), (10), the left-biased WENO approximation of $u_x(x_i)$ is defined as the following weighted average:

$$u_{x,i}^- = \omega_1 u_{x,i}^{-1} + \omega_2 u_{x,i}^{-2} + \omega_3 u_{x,i}^{-3} \tag{11}$$

where the weights $\omega_1 + \omega_2 + \omega_3 = 1$ are to be selected so that:

i. If the function u(x) is smooth in the combined six-point stencil $S^- = \{x_{i-3}, x_{i-2}, x_{i-1}, x_i, x_{i+1}, x_{i+2}\}$ then

$$\omega_1 = \frac{1}{10} + O(h^3) \quad \omega_2 = \frac{3}{5} + O(h^3) \quad \omega_3 = \frac{3}{10} + O(h^3) \tag{12}$$

ii. If the function u(x) contains a singularity or a steep gradient in the stencil $S_j^-$, and is smooth in at least one of the other two stencils, then

$$\omega_j = 0 + O(h^3) \tag{13}$$

The above two requirements entail that in regions where the function $u(x)$ is smooth the left-biased WENO approximation (11) renders a non oscillatory (at least ) fifth-order accurate deriva-

tive.

$$u_x^-(x_i) = \frac{1}{30}\frac{\Delta^+ u_{i-3}}{h} - \frac{13}{60}\frac{\Delta^+ u_{i-2}}{h} + \frac{47}{60}\frac{\Delta^+ u_{i-1}}{h} + \frac{9}{20}\frac{\Delta^+ u_i}{h} - \frac{1}{20}\frac{\Delta^+ u_{i+1}}{h} + O(h^5) \tag{14}$$

On the other hand, in regions where the function $u(x)$ contains a singularity or a steep gradient, the left biased WENO approximation (11) renders a nonoscillatory (at least) third-order accurate derivative.

Sets of weights that are consistent with the above two requirements are not unique. In this work, we shall make use of weights within the class of those proposed by Jiang and Shu (1996) in the context of the conservation laws. They are defined as follows:

$$\omega_j = \frac{\tilde{\omega}_j}{\tilde{\omega}_1 + \tilde{\omega}_2 + \tilde{\omega}_3} \text{ with } \tilde{\omega}_j = \frac{\gamma_j}{(\epsilon + S_j)^2} \qquad j = 1, 2, 3, \tag{15}$$

where

$$\gamma_1 = \frac{1}{10} \quad \gamma_2 = \frac{3}{5} \quad \gamma_3 = \frac{3}{10} \tag{16}$$

where

$$\begin{aligned}
S_1^- &= \sum_{l=2}^{3} h^{2l-1} \int_{x_i-\frac{1}{2}}^{x_i+\frac{1}{2}} \left(\frac{d^l p_1^-}{dx^l}\right)^2 dx = \frac{13}{12}(\Delta^-\Delta^+ u_{i-2} - \Delta^-\Delta^+ u_{i-1})^2 + (\Delta^-\Delta^+ u_{i-2} - 2\Delta^-\Delta^+ u_{i-1})^2 \\
S_2^- &= \sum_{l=2}^{3} h^{2l-1} \int_{x_i-\frac{1}{2}}^{x_i+\frac{1}{2}} \left(\frac{d^l p_2^-}{dx^l}\right)^2 dx = \frac{13}{12}(\Delta^-\Delta^+ u_{i-1} - \Delta^-\Delta^+ u_i)^2 + (\Delta^-\Delta^+ u_i)^2 \\
S_3^- &= \sum_{l=2}^{3} h^{2l-1} \int_{x_i-\frac{1}{2}}^{x_i+\frac{1}{2}} \left(\frac{d^3 p_2^-}{dx^l}\right)^2 dx = \frac{13}{12}(\Delta^-\Delta^+ u_i - \Delta^-\Delta^+ u_{i+1})^2 + (\Delta^-\Delta^+ u_i)^2
\end{aligned} \tag{17}$$

and the notation $\Delta^- v_k = v_k - v_{k-1}$ has been utilized for subsequent convenience. In $(15)_2$, $\epsilon$ is a small real number which is introduced to avoid vanishingly small denominators; for the types of pdes of interest here, numerical test indicated that $\epsilon = 10^{-6}$ is an adequate choice. The parameters $S_j^-$ defined by (17) are smoothness indicators: the larger the value of $S_j^-$, the lesser the smoothness of the function $u(x)$ in the stencil $S_j^-$. Note that these smoothness indicators are scaled sums of the square $L^2$-norms of the second and third derivatives of the corresponding interpolant on a stencil. The interested reader is referred to Jiang and Shu (1996) and Henrick et a1. (2005) for more details about the above and other weights.

Granted the choice of weights (15)-(17), the left-biased WENO approximation (11) of $u_x(x_i)$ can be rewritten in the more compact form

$$u^-_{x,i} = \frac{1}{12}\left( -\frac{\Delta^+ u_{i-2}}{h} + 7\frac{\Delta^+ u_{i-1}}{h} + 7\frac{\Delta^+ u_i}{h} - \frac{\Delta^+ u_{i+1}}{h}\right) - U\left(\frac{\Delta^-\Delta^+ u_{i-2}}{h}, \frac{\Delta^-\Delta^+ u_{i-1}}{h}, \frac{\Delta^-\Delta^+ u_i}{h}, \frac{\Delta^-\Delta^+ u_{i+1}}{h}\right) \quad (18)$$

where

$$U(z_1, z_2, z_3, z_4) = \frac{1}{3}\breve{\omega}_1(z_1 - 2z_2 + z_3) + \frac{1}{6}(\breve{\omega}_3 - \frac{1}{2})(z_2 - 2z_3 + z_4) \quad (19)$$

with

$$\breve{\omega}_1 = \frac{\frac{1}{10(\epsilon+\breve{S}_1)^2}}{\frac{1}{10(\epsilon+\breve{S}_1)^2} + \frac{3}{5(\epsilon+\breve{S}_2)^2} + \frac{3}{10(\epsilon+\breve{S}_3)^2}}, \quad \breve{\omega}_3 = \frac{\frac{3}{10(\epsilon+\breve{S}_3)^2}}{\frac{1}{10(\epsilon+\breve{S}_1)^2} + \frac{3}{5(\epsilon+\breve{S}_2)^2} + \frac{3}{10(\epsilon+\breve{S}_3)^2}} \quad (20)$$

$$\breve{S}_1 = \frac{13}{12}h^2(z_1 - z_2)^2 + h^2(z_1 - 2z_2)^2, \;\; \breve{S}_2 = \frac{13}{12}h^2(z_2 - z_3)^2 + h^2 z_3^2, \;\; \breve{S}_3 = \frac{13}{12}h^2(z_3 - z_4)^2 + h^2 z_3^2 \quad (21)$$

The right-biased WENO approximation. From symmetry arguments, given the four-point stencils $S_1^+ = \{x_i, x_{i+1}, x_{i+2}, x_{i+3}\}$, $S_2^+ = \{x_{i-1}, x_i, x_{i+1}, x_{i+2}\}$, $S_3^+ = \{x_{i-2}, x_{i-1}, x_i, x_{i+1}\}$, and the combined six-point stencil $S^+ = \{x_{i-2}, x_{i-1}, x_i, x_{i+1}, x_{i+2}, x_{i+3}\}$, it follows that the right-biased WENO approximation of $u_x(x_i)$ can be written as

$$u^+_{x,i} = \frac{1}{12}\left( -\frac{\Delta^+ u_{i-2}}{h} + 7\frac{\Delta^+ u_{i-1}}{h} + 7\frac{\Delta^+ u_i}{h} - \frac{\Delta^+ u_{i+1}}{h}\right) - U\left(\frac{\Delta^-\Delta^+ u_{i+2}}{h}, \frac{\Delta^-\Delta^+ u_{i+1}}{h}, \frac{\Delta^-\Delta^+ u_i}{h}, \frac{\Delta^-\Delta^+ u_{i-1}}{h}\right) \quad (22)$$

where it is recalled that the function U is defined by expressions (19) with (20)-(21).

### 2.1.2 WENO approximation of the partial derivatives of a multivariable function $\mathbf{u(x_1, x_2, ..., x_d)}$

The WENO approximation of the partial derivatives of a funtion of multiple variables $u(x_1, x_2, ..., x_d)$ can be readly generated in a dimension by dimension fashion in a Cartesian grid, with the one-variable procedure discussed in the previous subsection used for each variable. For simplicity of exposition let us consider functions of two variables $u(x_1, x_2)$ and let us write (x,y) rather than $(x_1, x_2)$. We denote by $x_i, y_j$ the (i,j) point in a grid with uniform spacing $h_x$ in the x-direction and $h_y$ in the y-direction. The left-biased WENO approximation of the partial derivatives $\frac{\partial u}{\partial x}(x_i, y_j)$ and $\frac{\partial u}{\partial y}(x_i, y_j)$ are then given, respectively, by the formulas

$$u^-_{x,i,j} = \frac{1}{12}\left( -\frac{\Delta^+_x u_{i-2,j}}{h_x} + 7\frac{\Delta^+_x u_{i-1,j}}{h_x} + 7\frac{\Delta^+_x u_{i,j}}{h_x} - \frac{\Delta^+_x u_{i+1,j}}{h_x}\right) - U\left(\frac{\Delta^-_x\Delta^+_x u_{i-2,j}}{h_x}, \frac{\Delta^-_x\Delta^+_x u_{i-1,j}}{h_x}, \frac{\Delta^-_x\Delta^+_x u_{i,j}}{h_x}, \frac{\Delta^-_x\Delta^+_x u_{i+1,j}}{h_x}\right) \tag{23}$$

and

$$u^-_{y,i,j} = \frac{1}{12}\left( -\frac{\Delta^+_y u_{i,j-2}}{h_y} + 7\frac{\Delta^+_y u_{i,j-1}}{h_y} + 7\frac{\Delta^+_y u_{i,j}}{h_y} - \frac{\Delta^+_y u_{i,j+1}}{h_y}\right) - U\left(\frac{\Delta^-_y\Delta^+_y u_{i,j-2}}{h_y}, \frac{\Delta^-_y\Delta^+_y u_{i,j-1}}{h_y}, \frac{\Delta^-_y\Delta^+_y u_{i,j}}{h_y}, \frac{\Delta^-_y\Delta^+_y u_{i,j+1}}{h_y}\right) \tag{24}$$

Similarly, the right-biased WENO approximation for the partial derivatives $\frac{\partial u}{\partial x}(x_i, y_i)$ and $\frac{\partial u}{\partial y}(x_i, y_i)$ are given by

$$u^+_{x,i,j} = \frac{1}{12}\left( -\frac{\Delta^+_x u_{i-2,j}}{h_x} + 7\frac{\Delta^+_x u_{i-1,j}}{h_x} + 7\frac{\Delta^+_x u_{i,j}}{h_x} - \frac{\Delta^+_x u_{i+1,j}}{h_x}\right) - U\left(\frac{\Delta^-_x\Delta^+_x u_{i+2,j}}{h_x}, \frac{\Delta^-_x\Delta^+_x u_{i+1,j}}{h_x}, \frac{\Delta^-_x\Delta^+_x u_{i,j}}{h_x}, \frac{\Delta^-_x\Delta^+_x u_{i-1,j}}{h_x}\right) \tag{25}$$

and

$$u^+_{y,i,j} = \frac{1}{12}\left( -\frac{\Delta^+_y u_{i,j-2}}{h_y} + 7\frac{\Delta^+_y u_{i,j-1}}{h_y} + 7\frac{\Delta^+_y u_{i,j}}{h_y} - \frac{\Delta^+_y u_{i,j+1}}{h_y}\right) - U\left(\frac{\Delta^-_y\Delta^+_y u_{i,j+2}}{h_y}, \frac{\Delta^-_y\Delta^+_y u_{i,j+1}}{h_y}, \frac{\Delta^-_y\Delta^+_y u_{i,j}}{h_y}, \frac{\Delta^-_y\Delta^+_y u_{i,j-1}}{h_y}\right) \tag{26}$$

respectively, where, analogous to the notation employed in the single-variable case, $\Delta^+_x v_{k,l} = v_{k+1,l} - v_{k,l}$, $\Delta^-_x v_{k,l} = v_{k,l} - v_{k-1,l}$, $\Delta^+_y v_{k,l} = v_{k,l+1} - v_{k,l}$, $\Delta^-_y v_{k,l} = v_{k,l} - v_{k,l-1}$, and where it is recalled that the function U is defined by expression (19) with (20)-(21). The corresponding formulae for functions of d variables should be now apparent.

### 2.2 The "space" discretization

Having introduced the space approximation to derivatives formulas of scalar-valued functions, we are now equipped to lay out the discretization of the Hamilton-Jacobi equations (1)-(2) in the "space" variables **F** and **E**. Before proceeding with the discretization per se, it proves convenient to rewrite the "space" variables **F** and **E** in component form and in the unified vectorial notation.

$$F_{11} = x_1,\ F_{22} = x_2,\ F_{33} = x_3,\ F_{12} = x_4,\ F_{21} = x_5,\ F_{13} = x_6,\ F_{31} = x_7,\ F_{23} = x_8,\ F_{32} = x_9,$$
$$E_1 = x_{10}\ E_2 = x_{11}\ E_3 = x_{12} \tag{27}$$

so that, with a slight abuse of notation, the Hamilton-Jacobi PDE (1) can be rewritten as

$$\frac{\partial W}{\partial c} + H\left(x_1, ..., x_{12}, c, w, \frac{\partial W}{\partial x_1}, ..., \frac{\partial W}{\partial x_{12}}\right) = 0 \qquad W(x_1, ..., x_{12}, 1) = W^{(2)}(x_1, ..., x_{12}) \tag{28}$$

where the Hamiltonian H is given by the expression (2) suitably rewritten in terms of the $x_i$ $i = 1, 2, ..., 12$ variables (27). For simplicity of exposition we shall present the scheme for Hamilton-Jacobi equations (1) - (2) that involve only two of these twelve $x_i$ variables and denote those by x and y, namely, with a slight abuse of notation again,

$$\frac{\partial W}{\partial c} + H\left(x, y, c, w, \frac{\partial W}{\partial x}, \frac{\partial W}{\partial y}\right) = 0 \qquad W(x, y, 1) = W^{(2)}(x, y) \tag{29}$$

The corresponding scheme for the general case when the Hamilton-Jacobi equation (28) involves all twelve $x_i$ variables will be clear from this special case, and we will not explicitly formulate it.

As aforementioned Crandall and Lions (1984) proved that first-order monotone schemes are convergent to the viscosity solution. Considering the "space" (x,y) to be discretized by a grid with uniform spacing $\Delta x$ in the x-direction and $\Delta y$ in the y-direction and denoting by $W_{i,j}$ the numerical approximation to the viscosity solution at the "space" point (x,y)=$(x_i, y_j)$ and "time" $c$, $W(x_i, y_j, c) = W(i\Delta x, j\Delta y, c)$ first-order monotone schemes refer to schemes of the form

$$\frac{\partial W_{i,j}}{\partial c} = -\hat{H}\left(x_i, y_j, c, \frac{\Delta_x^+ W_{i,j}}{\Delta x}, \frac{\Delta_x^- W_{i,j}}{\Delta x}, \frac{\Delta_y^+ W_{i,j}}{\Delta y}, \frac{\Delta_y^- W_{i,j}}{\Delta y}\right) \tag{30}$$

where $\hat{H}$ is the so called numerical Hamiltonian (also termed flux) which is a Lipschitz continuous function that has to be consistent and monotone. Consistency with respect to the discrete forward and backward derivatives is

$$\hat{H}(x, y, c, W, p, p, q, q) = H(x, y, c, W, p, q) \tag{31}$$

monotonicity in terms of the forward and backward derivative means that the numerical Hamiltonian is a non increasing function in its fifth and seventh argument and nondecreasing in its sixth and eight arguments, symbolically

$$\hat{H}(x, y, c, W, \downarrow, \uparrow, \downarrow, \uparrow) \tag{32}$$

There is a considerable number of monotone numerical Hamiltonians proposed in the literature (see. e.g., Osher and Shu 1991: Kurganov et a1., 2001). Mentioning some of the most well know monotonic numerical Hamiltonian, where the dependence in $(x, y, c)$ is omitted to ease notation.

(1) The local Lax Friedrich (LLF) flux is

$$\hat{H}^{LLF}(p^+, p^-, q^+, q^-) = H\left(\frac{p^+ + p^-}{2}, \frac{q^+ + q^-}{2}\right) - \nu_1(p^+, p^-)\frac{p^+ - p^-}{2} - \nu_2(q^+, q^-)\frac{q^+ - q^-}{2} \quad (33)$$

with

$$\nu_1(p^+, p^-) = \max_{\substack{p \in I(p^-, p^+) \\ q \in [C,D]}} |H_1(p, q)| \qquad \nu_2(q^+, q^-) = \max_{\substack{q \in I(q^-, q^+) \\ p \in [A,B]}} |H_2(p, q)| \quad (34)$$

$H_1$ and $H_2$ are partial derivatives of H with respect to $u_x$ and $u_y$ respectively. [A, B] are the range of values of $p^{\pm}$ and [C, D] the range of values for $q^{\pm}$. The operation $I(a, b)$ is equal to $I(a, b) = [min(a, b), max(a, b)]$.

(2) Roe flux with LLF entropy

$$\hat{H}(p^+, p^-, q^+, q^-) = \begin{cases} H(p^*, q^*) & \text{if } H_1(p,q) \text{ and } H_2(p,q) \text{ do not change signs in p} \in I(p^+, p^-), \text{ q} \in I(q^+, q^-) \\ H(\frac{p^+ + p^-}{2}, q^*) - \nu_1(p^+, p^-)\frac{p^+ - p^-}{2} & \text{otherwise and if } H_2(p,q) \text{ does not change sign in } A \le p \le B, \quad \text{q} \in I(q^+, q^-) \\ H(p^*, \frac{q^+ + q^-}{2}) - \nu_2(q^+, q^-)\frac{q^+ - q^-}{2} & \text{otherwise and if } H_1(p,q) \text{ does not change sign in p} \in I(p^+, p^-), \quad C \le q \le D, \\ \hat{H}^{LLF}(p^+, p^-, q^+, q^-) & otherwise \end{cases} \quad (35)$$

where $p^*$ and $q^*$ are defined by

$$p^* = \begin{cases} p^+ & \text{if } H_1(p,q) \le 0 \\ p^- & \text{if } H_1(p,q) \ge 0 \end{cases} \qquad q^* = \begin{cases} q^+ & \text{if } H_2(p,q) \le 0 \\ q^- & \text{if } H_2(p,q) \ge 0 \end{cases} \quad (36)$$

Here $H_1 = \partial H(p,q)/\partial p$, $H_2 = \partial H(p,q)/\partial q$, [A,B] ([C D]) denote the ranges of values taken

by $p^{\pm}$ ($q^{\pm}$) over the entire considered "space" (x,y). The rationale behind this choice of numerical Hamiltonian is twofold. It has been successfully utilized in a variety of hyperbolic conservation laws and Hamilton-Jacobi equations (see, e.g. Osher and Fedkiw, 2003). Further, its implementation (for any number of "space" variables) in a numerical code is straightforward.

### 2.3 "Time" discretization

For the time discretization of the Hamilton-Jacobi equation we recur to a fifth-order Runge-Kutta discretization with extended region of stability proposed by Lawson(1966). Shu and Osher (1988) recognized that this discretization is among within the class that would latter be known as strong stability preserving (SSP) Runge-Kutta methods (Gottlieb et. a1. 2001). The time is also discretized in Cartesian grid $c_n = n\Delta c$. Making use of the same notation from the beginning we have that $W(x_i, y_j, c_n) = W(i\Delta x, j\Delta y, n\Delta c)$, is the discretized value of $W$ at $(x_i, y_j, c_n)$. The algorithm to compute $W_{i,j}^{n+1}$ with $W_{i,j}^{n}$ reads as follow. Define

$$L_{i,j}^{(l)} = -\hat{H}(x_i, y_j, c_n, W_{i,j}^{l}, W_{x,i,j}^{l+}, W_{x,i,j}^{l-}, W_{y,i,j}^{l+}, W_{y,i,j}^{l-}) \tag{37}$$

where again, the numerical Hamiltonian $\hat{H}$ is given by the Roe Flux or Local Lax Friedrich flux, $W_{x,i,j}^{l+}$, $W_{x,i,j}^{l-}$, $W_{y,i,j}^{l+}$, $W_{y,i,j}^{l-}$ are the fifth-order approximation (23)-(26), we obtain $W_{i,j}^{n+1}$ from $W_{i,j}^{n}$ by following the fifth-oder Runge-Kutta procedure:

$$\begin{aligned}
W_{i,j}^{(1)} &= W_{i,j}^{(n)}, & k_{i,j}^{(1)} &= L_{i,j}^{(1)}(c^n) \\
W_{i,j}^{(2)} &= W_{i,j}^{(1)} + \frac{\Delta c}{2} k_{i,j}^{(1)}, & k_{i,j}^{(2)} &= L_{i,j}^{(2)}\left(c^n + \frac{\Delta c}{2}\right) \\
W_{i,j}^{(3)} &= W_{i,j}^{(1)} + \frac{\Delta c}{16}(3k_{i,j}^{(1)} + k_{i,j}^{(2)}), & k_{i,j}^{(3)} &= L_{i,j}^{(3)}\left(c^n + \frac{\Delta c}{4}\right) \\
W_{i,j}^{(4)} &= W_{i,j}^{(1)} + \frac{\Delta c}{2} k_{i,j}^{(3)}, & k_{i,j}^{(4)} &= L_{i,j}^{(4)}\left(c^n + \frac{\Delta c}{2}\right) \\
W_{i,j}^{(5)} &= W_{i,j}^{(1)} + \frac{3\Delta c}{16}(-k_{i,j}^{(2)} + 2k_{i,j}^{(3)} + 3k_{i,j}^{(4)}), & k_{i,j}^{(5)} &= L_{i,j}^{(5)}\left(c^n + \frac{3\Delta c}{4}\right) \\
W_{i,j}^{(6)} &= W_{i,j}^{(1)} + \frac{\Delta c}{7}(k_{i,j}^{(1)} + 4k_{i,j}^{(2)} + 6k_{i,j}^{(3)} - 12k_{i,j}^{(4)} + 8k_{i,j}^{(5)}), & k_{i,j}^{(6)} &= L_{i,j}^{(6)}(c^n + \Delta c) \\
W_{i,j}^{(n+1)} &= W_{i,j}^{(n)} + \frac{\Delta c}{90}(7k_{i,j}^{(1)} + 32k_{i,j}^{(3)} + 12k_{i,j}^{(4)} + 32k_{i,j}^{(5)} + 7k_{i,j}^{(6)})
\end{aligned} \tag{38}$$

The following remarks are in order:

i. The developed scheme is formally fifth-order accurate in "space" and "time" in regions far from steep gradients.

ii. The Runge-Kutta time discretization recently shown can be proven SSP under Courant-Friedrichs-Levy-CFL condition

$$|\Delta c| \leq \frac{7}{30}|\Delta c_{FE}| \tag{39}$$

if the first order-forward and backward Euler time discretization $W_{i,j}^{n+1} = W_{i,j}^{n} \pm \Delta c\, L_{i,j}^{n}(c^n)$ are SSP under CFL condition

$$|\Delta c| \leq \frac{7}{30}|\Delta c_{FE}| \tag{40}$$

with

$$|\Delta c_{FE}|\, max\left\{ \frac{|H_1|}{\Delta x} + \frac{|H_2|}{\Delta y} \right\} \leq 1 \tag{41}$$

see Lemma 2.2. in Gottlieb et a1. (2001).

iii. The physical requirement of material impenetrability imposes the restriction that the free energy functions $W^{(1)}$ and $W^{(2)}$ describing the elastic dielectric behaviors of the underlying matrix and particles must be such $W^{(1)}(\mathbf{F},\mathbf{E})$, $W^{(2)}(\mathbf{F},\mathbf{E}) \to \infty$ as $\det\mathbf{F} \to 0+$. Because of other constitutive requirements, $W^{(1)}(\mathbf{F},\mathbf{E})$ and $W^{(2)}(\mathbf{F},\mathbf{E})$ may also become unbounded (from above and/or from below) at certain values of $\mathbf{F}$ and $\mathbf{E}$. This implies that the ($\mathbf{F}$,$\mathbf{E}$) "space" domain over which the viscosity solution of (1)-(2) remains finite ranges from semi-infinite to bounded, depending on the specific nature of the free energy function $W^{(1)}$ and $W^{(2)}$. In turn, this implies that care must be exercised in the implementation of the developed scheme to deal with boundary conditions.

Given that implicit integration schemes are generally more stable, a semi implicit integration method is proposed. A fully implicit integration method with the non-linear weights inside the iteration would present an excessive computer cost that is why the weights are calculated with a third order explicit runge kutta

$$\begin{aligned}
W_{i,j}^{(1)} &= W_{i,j}^{(n)}, & k_{i,j}^{(1)} &= L_{i,j}^{(1)}(c^n) \\
W_{i,j}^{(2)} &= W_{i,j}^{(1)} + \Delta c\, k_{i,j}^{(1)}, & k_{i,j}^{(2)} &= L_{i,j}^{(2)}\left(c^n + \Delta c\right) \\
W_{i,j}^{(3)} &= W_{i,j}^{(1)} + \frac{\Delta c}{4}(k_{i,j}^{(1)} + k_{i,j}^{(2)}), & k_{i,j}^{(3)} &= L_{i,j}^{(3)}\left(c^n + \frac{\Delta c}{2}\right) \\
W_{i,j}^{p} &= W_{i,j}^{(1)} + \frac{\Delta c}{6}(k_{i,j}^{(1)} + k_{i,j}^{(2)} + 4k_{i,j}^{(3)}), & &
\end{aligned} \tag{42}$$

the nonlinear weights for each grid point are then obtained with

$$\omega_j^p = \omega_j^p(W^p) \tag{43}$$

And finally using these predictor weights the implicit integration step is carried out

$$W_{i,j}^{(n+1)} = W_{i,j}^{(n)} + \frac{1}{2}\Delta c\left(k_{i,j}^{(1)} + k_{i,j}^{(2)}\right);$$
$$k_{i,j}^{(1)} = L_{i,j}^{(1)} = L_{i,j}^{(n)}(c^n, \omega_j); \quad k_{i,j}^{(2)} = L_{i,j}^{(n+1)}(c^n + \Delta c, \omega_j^p) \tag{44}$$

## 2.4 Boundary treatment

### 2.4.1 Lagrange type extrapolation

Because of the wide stencil of the interior high order scheme a treatment of the boundary is needed. Near the boundary the forward and backward derivatives need points that are out of the computational domain. There is a reduced number of works in the subject, Sirui Tan and Chi-Wang Shu (2010) and Sirui Tan et a1 (2011) treated the problem by introducing ghost points outside the computational boundary. For the scheme of the paper we propose a type of lagrange extrapolation in the derivatives. In a way to illustrate the procedure this is done for a single space variable, where the forward and backward derivatives are (if the function $u$ is smooth)

$$p_i^- = u_{x,i}^- = \frac{1}{60h}(-2u_{i-3} + 15u_{i-2} - 60u_{i-1} + 20u_i + 30u_{i+1} - 3u_{i+2}) \tag{45}$$
$$p_i^+ = u_{x,i}^+ = \frac{1}{60h}(3u_{i-2} - 30u_{i-1} - 20u_i + 60u_{i+1} - 15u_{i+2} + 2u_{i+3}) \tag{46}$$

As mentioned previously in the last and first three points of the computational domain the forward and backward derivatives would need points that are not in the computational domain. Assuming a lagrange type polynomial approximation for the derivative where the wide derivatives are completely defined.

$$L^+(x) = \sum_{j=k}^{n} p_j^+ l_j(x) \tag{47}$$

with n representing the order of extrapolation and $l_j$ are the lagrange polynomials equal to

$$l_j(x) = \prod_{\substack{1 \le m \le k \\ m \ne j}} \frac{x - x_m}{x_j - x_m} \tag{48}$$

Then the derivatives in the computational boundary are extrapolated with each polynomial. Using a quadratic Lagrange polynomial for the extrapolation of the first three points

$$L^+(x) = p_4^+ l_4(x) + p_5^+ l_5(x) + p_6^+ l_6(x) \tag{49}$$

for the last three points respectively

$$L^+(x) = p^+_{N-5} l_{N-5}(x) + p^+_{N-4} l_{N-4}(x) + p^+_{N-3} l_{N-3}(x) \tag{50}$$

where $N$ is the total number of points of the discretization. This process can be easily extended for the backward derivatives and for any dimension.

# 3 Assessment of convergence and stability

## 3.1 Hamilton-Jacobi equations to solve

In the sequel we investigate the convergence and stability of the above-developed scheme to solve Hamilton-Jacobi equations of the class (1)-(2) by means of a physically based problems: the overall elastic in plane response of a Gaussian elastomer weakened by a transversely isotropic distribution of spherical vacuous pores, under two different types of loading. The first loading path that we investigate is an hydrostatic deformation

$$\mathbf{F} = \mathrm{diag}(\lambda, \lambda, \lambda) \qquad\qquad \mathbf{E} = \mathbf{0} \tag{51}$$

the matrix and particles are characterized by the free energy functions

$$W^{(1)}(\mathbf{F}, \mathbf{0}) = \begin{cases} \frac{\mu}{2}\left[\mathbf{F}\cdot\mathbf{F} - 3\right] & if\ det\mathbf{F} = 1 \\ \infty & otherwise \end{cases} \tag{52}$$

$$W^{(1)}(\mathbf{F}, \mathbf{0}) = 0 \tag{53}$$

Which results in an ODE

$$\frac{\partial W}{\partial c} + H\left(J, c, W, \frac{\partial W}{\partial J}\right) = 0 \qquad W(J, 1) = 0 \tag{54}$$

$$H = (J-1)\frac{\partial W}{\partial J} + \frac{\mu}{2}\left(2J^{2/3} + \frac{1}{J^{4/3}} - 3\right) \tag{55}$$

where J is the determinant of the deformation gradient equal to $J = \lambda^3$. The exact solution is given by the analytical equation

$$W = \frac{3\mu}{2}\left[\frac{2J-1}{J^{1/3}} - \frac{2J+c-2}{(J+c-1)^{1/3}}c^{1/3} - (1-c)\right] \tag{56}$$

The second loading path corresponds to a plane deformation where the deformation gradient and electrical field are setted as

$$\mathbf{F} = \mathrm{diag}(\lambda_1, \lambda_2, 1) \qquad\qquad \mathbf{E} = \mathbf{0} \tag{57}$$

Under the above assumption and the same material behaviors for the matrix and particles the Hamilton-Jacobi equation that is obtained is

$$\frac{\partial W}{\partial c}+H\left(\lambda_1,\lambda_2,c,W,\frac{\partial W}{\partial \lambda_1},\frac{\partial W}{\partial \lambda_2}\right)=0 \qquad W(\lambda_1,\lambda_2,1)=0 \tag{58}$$

where the Hamiltonian is equal to

$$\begin{aligned} H=&-\frac{1}{c}W+\frac{2+\lambda_1\lambda_2(\lambda_1^2+\lambda_2^2-4)}{4c\lambda_1\lambda_2}\mu+\frac{\lambda_1^2+\lambda_1\lambda_2-2}{2c(\lambda_1+\lambda_2)}\frac{\partial W}{\partial \lambda_1}+\frac{\lambda_2^2+\lambda_1\lambda_2-2}{2c(\lambda_1+\lambda_2)}\frac{\partial W}{\partial \lambda_1}\\ &-\frac{\lambda_1^2}{4c\mu(\lambda_1+\lambda_2)}\left(\frac{\partial W}{\partial \lambda_1}\right)^2-\frac{\lambda_2^2}{4c\mu(\lambda_1+\lambda_2)}\left(\frac{\partial W}{\partial \lambda_2}\right)^2+\frac{\lambda_1\lambda_2}{2c\mu(\lambda_1+\lambda_2)}\frac{\partial W}{\partial \lambda_1}\frac{\partial W}{\partial \lambda_2} \end{aligned} \tag{59}$$

quite exceptional is that the solution of the Hamilton-Jacobi equation (58) - (59) for any value of initial volume fraction of cylindrical pores $c \in [0,1]$, can be written in closed form (Lopez-Pamies and Idiart, 2009). The result reads as

$$W=\frac{\mu}{2}\frac{1-c}{1+c}\left[\lambda_1^2+\lambda_2^2-2\right]+\frac{\mu}{2}(\lambda_1\lambda_2-1)\ \left[ln\left(\frac{\lambda_1\lambda_2+c-1}{c\lambda_1\lambda_2}\right)-2\frac{1-c}{1+c}\right] \tag{60}$$

Remark 1. The effective free energy function (60) is a symmetric function of its "space" variables, namely, $W(\lambda_2,\lambda_1,c)=W(\lambda_1,\lambda_2,c)$ . Only computation in the domain $\lambda_2 \leq \lambda_1$ is needed

Remark 2. The effective free energy function (60) becomes unbounded at deformations with $\lambda_1\lambda_2=1-c$. Physically, this is a manifestation of the fact that, for an incompressible elastomer with initial volume fraction of pores $c$, the volume fraction of pores in the deformed configuration vanishes whenever $J=1-c$, and further volume reducing deformations require infinite energy. Computationally this implies that special care must be exercised near the boundary "space" - "time" boundary $\lambda_1\lambda_2=1-c$. Taking into account for the previously mentioned boundary condition, we recur to a change of variables

$$\Lambda=\frac{\lambda_2}{\lambda_1}; \qquad J=\lambda_1\lambda_2 \tag{61}$$

the Hamilton-Jacobi equation can ve rewritten as

$$\frac{\partial \hat{W}}{\partial c}+H\left(\Lambda,J,c,\hat{W},\frac{\partial \hat{W}}{\partial \Lambda},\frac{\partial \hat{W}}{\partial J}\right)=0; \qquad \hat{W}(\Lambda,J,1)=0 \tag{62}$$

with Hamiltonian

$$H=-\frac{\hat{W}}{c}+\frac{\mu}{c}\left[\frac{J}{4}\left(\Lambda+\frac{1}{\Lambda}\right)+\frac{1}{2J}-1\right]+\frac{(\Lambda-1)\Lambda}{c(\Lambda+1)J}\frac{\partial \hat{W}}{\partial \Lambda}+\frac{(J-1)}{c}\frac{\partial \hat{W}}{\partial J}-\frac{\Lambda^3}{c(\Lambda+1)^2J\mu}\left(\frac{\partial \hat{W}}{\partial \Lambda}\right)^2 \tag{63}$$

this representation is more convenient at the time of dealing with the compressibility restriction of Remark 2. Given that in this space of variables the unbounded deformations appears at $J = 1 - c$ and thus in a Cartesian grid this boundary space constitutes a line of points of the grid for each "time" $c$.

### 3.2 Change of variables

The kind of Hamilton-Jacobi equations that we want to solve has new challenges, from which the non-artificial boundary conditions (non-periodic boundary conditions) is the most significant. Because of this, an extrapolation has to be used given the wide stencil. This extrapolation at the same time causes errors specially where steep gradients are located, errors that propagate from the boundary and can cause stability problems. Just by using a marching method with the original coordinates (61), it was observed that the errors of the boundary caused the scheme to be unstable, that is why a change of variables was proposed which stretches space and time.

$$t = -log_\tau c \quad ; \quad \check{J} = log_x J; \tag{64}$$

the new PDE to solve is then

$$\frac{\partial \check{W}}{\partial c} + H\left(\check{J}, c, \check{W}, \frac{\partial \check{W}}{\partial \check{J}}\right) = 0 \qquad \check{W}(J,1) = 0 \tag{65}$$

$$H = \frac{(J-1)}{J}\frac{\partial \check{W}}{\partial \check{J}} + \frac{\mu}{2}\left(2J^{2/3} + \frac{1}{J^{4/3}} - 3\right) = 0 \qquad \check{W}(J,1) = 0 \tag{66}$$

Making use of an analogous change of variables for the second loading path

$$t = -log_\tau c, \qquad \check{\lambda}_1 = log_x\, \lambda_1, \qquad \check{\lambda}_2 = log_x\, \lambda_2, \tag{67}$$

the new PDE to solve is then

$$\frac{\partial \tilde{W}}{\partial t} + H\left(\check{\lambda}_1, \check{\lambda}_2, t, \tilde{W}, \frac{\partial \tilde{W}}{\check{\lambda}_1}, \frac{\partial \tilde{W}}{\check{\lambda}_2}\right) = 0 \qquad \tilde{W}(\check{\lambda}_1, \check{\lambda}_2, 1) = 0 \tag{68}$$

with Hamiltonian

$$\begin{aligned} H = \ln\tau\Bigg(\tilde{W} - \frac{2 + \lambda_1\lambda_2\,(\lambda_1^2 + \lambda_2^2 - 4)}{4c\lambda_1\lambda_2}\mu - \frac{\lambda_1^2 + \lambda_1\lambda_2 - 2}{2c\,\ln x\;\lambda_1(\lambda_1 - \lambda_2)}\frac{\partial \tilde{W}}{\partial \check{\lambda}_1} + \frac{\lambda_2^2 + \lambda_1\lambda_2 - 2}{2c\,\ln x\;\lambda_2(\lambda_1 + \lambda_2)}\frac{\partial \tilde{W}}{\partial \check{\lambda}_2} \\ - \frac{\lambda_1^2}{4c(\ln x)^2\,\lambda_1^2\mu(\lambda_1 + \lambda_2)}\left(\frac{\partial \tilde{W}}{\partial \check{\lambda}_1}\right)^2 - \frac{\lambda_2^2}{4c(\ln x)^2\lambda_2^2\mu(\lambda_1 + \lambda_2)}\left(\frac{\partial \tilde{W}}{\partial \check{\lambda}_1}\right)^2 \\ \frac{\lambda_1\lambda_2}{2c\,(\ln x)^2\,\lambda_1\lambda_2\,\mu\,(\lambda_1 + \lambda_2)}\frac{\partial \tilde{W}}{\partial \check{\lambda}_1}\frac{\partial \tilde{W}}{\partial \check{\lambda}_2}\Bigg) \end{aligned} \tag{69}$$

For the variables Λ, J

$$t = -log_{\tau} c \qquad \check{\Lambda} = log_x \Lambda; \qquad \check{J} = log_x J; \tag{70}$$

$$\frac{\partial \check{W}}{\partial t} + H\left(\check{\Lambda}, \check{J}, t, \check{W}, \frac{\partial \check{W}}{\partial \check{\Lambda}}, \frac{\partial \check{W}}{\partial \check{J}}\right) = 0 \qquad \check{W}(\check{\Lambda}, \check{J}, 1) = 0 \tag{71}$$

with Hamiltonian

$$\begin{aligned} H &= \ln\tau \left( - \check{W} + \mu \left[ \frac{J}{4}\left(\Lambda + \frac{1}{\Lambda}\right) + \frac{1}{2J} - 1 \right] + \frac{\Lambda(\Lambda - 1)}{(\Lambda + 1)\ J\ \Lambda\ \ln x} \frac{\partial \check{W}}{\partial \check{\Lambda}} \right. \\ &\quad \left. + \frac{J-1}{J\ \ln x} \frac{\partial \check{W}}{\partial \check{J}} - \frac{\Lambda^3}{(\Lambda+1)^2 \Lambda^2 (\ln x)^2 J \mu} \left( \frac{\partial \check{W}}{\partial \check{\Lambda}} \right)^2 \right) \end{aligned} \tag{72}$$

## 3.3 Results

### 3.3.1 Results for the hydrostatic loading path

From Figures 1 and 2, it can be seen that for both integration methods explicit and implicit as the integration begins at "time" zero or at a concentration of one ($c$=1), mesh refinement improves accuracy. However, as "time" progresses or as the concentration reaches one, the accuracy for different meshes approaches one another. When a implicit integration method is carried out, we can see that the difference between different meshes remains a longer "time". The step time is fixed as a power of the grid space $\Delta t = (\Delta x)^p$ with $p \in \mathbb{N}$. The values of the accuracy remain more or less similar for different step times, this is a similar result to what is obtained for the standard test problem (Butcher 1987), problem that consist in solving the ODE $y' = ky$, $k \in \mathbb{C}$ numerically, for this problem using Runge kutta methods there is a stability region or a step time for which the method is stable for larger step times the explicit integration method turns out to be unstable. Figure 1 seems to indicate that the accuracy does not change by reducing the step time once the scheme is stable.

On the other hand, from Figure 2 one can observe that with implicit integration the accuracy improves as the step time diminish. The convergence rates shown in Figures 3 - 4 also reflect an analogous behavior, by decreasing the step time the convergence for the explicit integration remains unaltered and improves for implicit integration. Ideally the method should always have a fifth order convergence, nevertheless, as "time" progresses and the concentration factor reaches zero the method is not fifth order anymore.

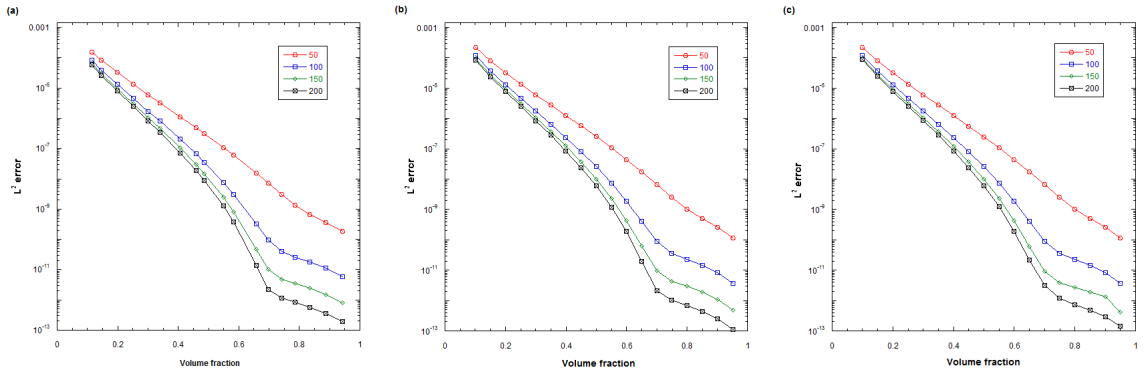


Figure 1: Accuracy plots for explicit time integration for different time steps (a) $\Delta t = \Delta x$, (b) $\Delta t = (\Delta x)^2$ and (c) to $\Delta t = (\Delta x)^3$

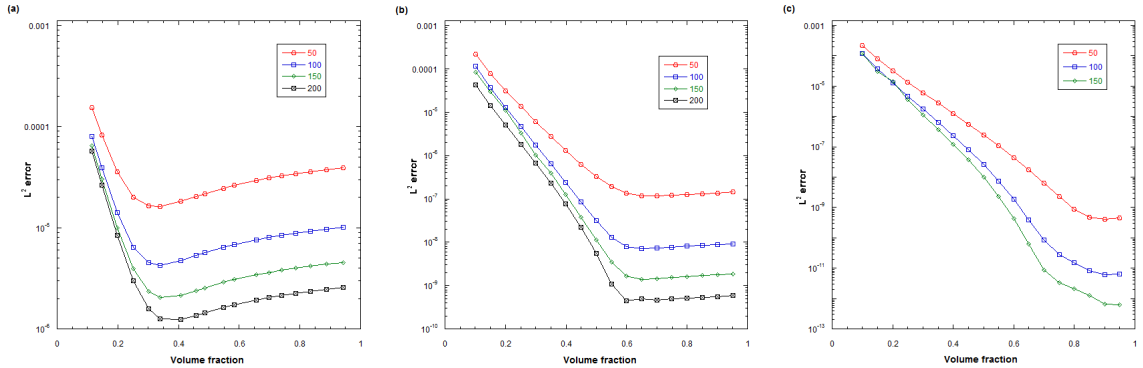


Figure 2: Accuracy plots for implicit time integration for different time steps (a) $\Delta t = \Delta x$, (b) $\Delta t = (\Delta x)^2$ and (c) to $\Delta t = (\Delta x)^3$

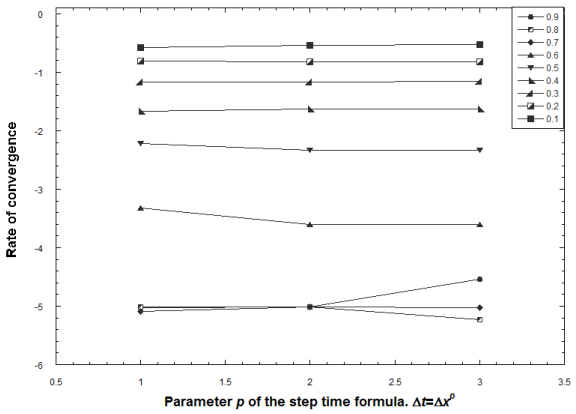


Figure 3: Rate of convergence vs different values of p, $\Delta t = (\Delta x)^p$. Explicit integration

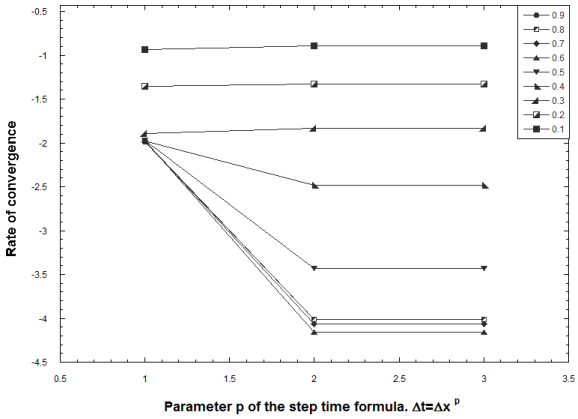


Figure 4: Rate of convergence vs different values of p, $\Delta t = (\Delta x)^p$. Implicit integration

### 3.3.2 Results for the planar deformation loading path

The results for the planar deformation loading path are similar to the previous loading path. For explicit integration the accuracy improves at the beginning of the integration time by reducing

the grid space; as time progresses the accuracy for different meshes approaches one another. With respect to implicit integration this behavior of improvement of accuracy by mesh refinement remains a longer "time", for example in Figure 6a this difference is maintained up to a twenty percent of concentration. By diminishing the step time the accuracy in the explicit integration case remains almost unchanged, and for the implicit integration improves, but for shorter interval of "time".

The convergence rates for a given concentration $c$ remain constant with the step time for explicit integration (as in the previous deformation path) Figure 7. In contrast for the implicit type of integration Figure 8, there seems to be a lost of convergence rate by diminishing the step time the reason of this could be that the extrapolation on the boundary adds errors and instabilities to the scheme at each step. Even more when an implicit integration is carried out and an algebraic non-linear system has to be solved which includes all the grid points, the smaller the step time the more operations are done –where the errors of the boundaries are included. On the whole the convergence rates for implicit integration are better than for explicit integration.

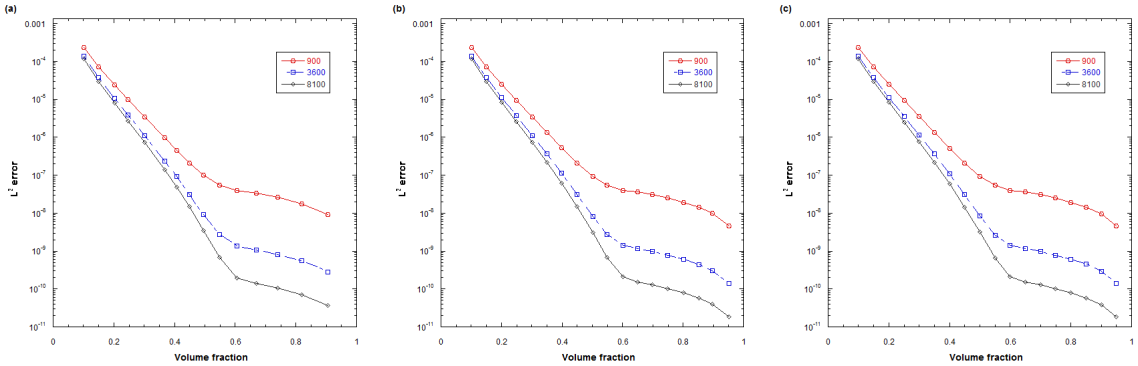


Figure 5: Accuracy plots for explicit time integration for different time steps (a) $\Delta t = \Delta x$, (b) $\Delta t = (\Delta x)^2$ and (c) to $\Delta t = (\Delta x)^3$

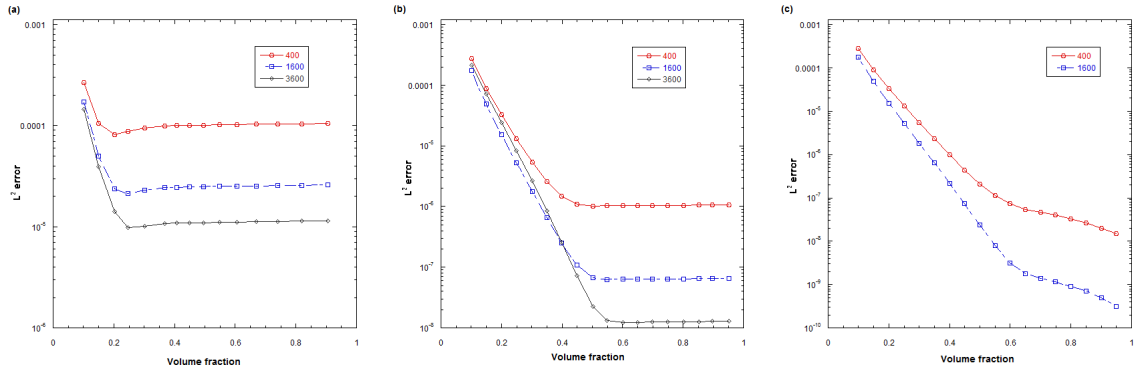


Figure 6: Accuracy plots for implicit time integration for different time steps (a) $\Delta t = \Delta x$, (b) $\Delta t = (\Delta x)^2$ and (c) to $\Delta t = (\Delta x)^3$

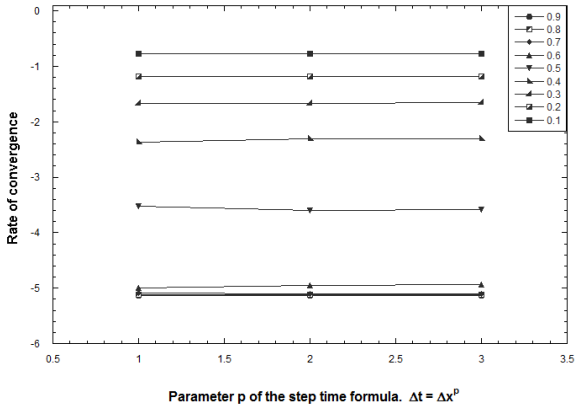


Figure 7: Rate of convergence vs different values of p, $\Delta t = (\Delta x)^p$. Explicit integration

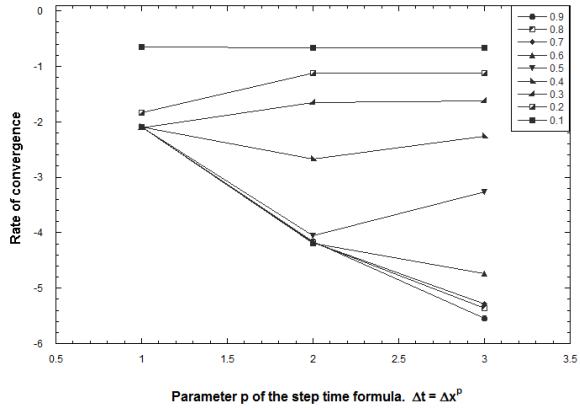


Figure 8: Rate of convergence vs different values of p, $\Delta t = (\Delta x)^p$. Implicit integration

### 3.4 Convergence and stability assessment conclusion

The WENO scheme was tested for Hamilton-Jacobi equations that arise from homogenization processes of a matrix weakened by spherical pores, under two different loading paths: planar and hydrostatic deformations loading paths, which correspond to a 1D and 2D space discretizations. Ideally speaking the scheme if the function is smooth should have fifth order convergence (see Jiang and Peng 2000). However, all the previous PDEs that were solved in the literature with these kind of marching methods —WENO and ENO schemes, for example— have periodic boundary conditions, the lack of these conditions seems to be the reason why instabilities appear in the boundary and there is a reduction of the convergence order.

A simple test was carried out about the role of the boundary conditions on the convergence behavior. The calculations were done for the hydrostatic loading path with an explicit time integration and then calculating the convergence rate using half of the Cartesian domain, the results are shown in Figure 9 where one can realize that the scheme remains fifth order accurate until very low concentration.

As previously shown in the plots for explicit integration the accuracy and convergence rate do not change by diminishing the step time. On the other hand, for implicit integration there seems to be an optimum step time for larger steps times the accuracy is not as good, and for smaller step times the errors at the boundary affect all the scheme. It can also be pointed out that for the optimum step time the convergence rates for implicit integration are better than for explicit, however, this kind of integration is more costly computationally .

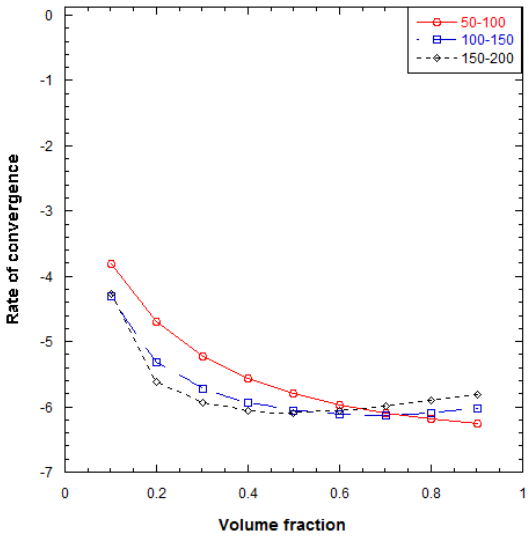


Figure 9: Fifth order convergence test

## 4 Application to isotropic porous elastomers

In this section as a first effort to illustrate the capabilities of the scheme, we deploy it to work out the overall elastic response of a Gaussian elastomer containing a random isotropic distribution of vacuous pores under arbitrary 3D deformations. We remark that Lopez-Pamies et a1. (2011b) had previously obtained an analytical result for this same problem in the limiting case of a dilute distribution of pores (i.e., for $c \to 0+$). Here, we work out results for the initial volume fractions of pores in the entire physical range $c \in [0,1]$. Thus, we consider the case when the macroscopic deformation gradient and electric field are of the form.

$$\mathbf{F} = \text{diag}(\lambda_1, \lambda_2, \lambda_3) \qquad \mathbf{E} = \mathbf{0} \tag{73}$$

the matrix and particles are characterized by the free energy function (52) and (53), and the microstructural function (3) is given by

$$\nu(\boldsymbol{\xi}) = \frac{1}{4\pi} \tag{74}$$

A schematic of the problem at hand is depicted by fig 1(b). Granted the electromechanical loading (73), matrix and particle behaviors (52)-(53), and micro structure function (74), lengthly but straightforward calculations show that the general Hamilton-Jacobi equation (1)-(2) in twelve "space" variables reduces to the following Hamilton-Jacobi equation in three "space" variables:

$$\frac{\partial W}{\partial c} + H\left(\lambda_1, \lambda_2, \lambda_3, c, W, \frac{\partial W}{\partial \lambda_1}, \frac{\partial W}{\partial \lambda_2}, \frac{\partial W}{\partial \lambda_3}\right) = 0 \qquad\qquad W(\lambda_1, \lambda_2, \lambda_3, 1) = 0 \tag{75}$$

with Hamiltonian

$$\begin{aligned} H \;=\; & -\frac{W}{c} + \frac{\mu\, G_0}{c} + \frac{G_1}{c}\frac{\partial W}{\partial \lambda_1} + \frac{G_2}{c}\frac{\partial W}{\partial \lambda_2} + \frac{G_3}{c}\frac{\partial W}{\partial \lambda_3} + \frac{G_4}{c\,\mu}\left(\frac{\partial W}{\partial \lambda_1}\right)^2 + \frac{G_5}{c\,\mu}\left(\frac{\partial W}{\partial \lambda_2}\right)^2 + \frac{G_6}{c\,\mu}\left(\frac{\partial W}{\partial \lambda_3}\right)^2 \\ & + \frac{G_7}{c\,\mu}\left(\frac{\partial W}{\partial \lambda_1}\right)\left(\frac{\partial W}{\partial \lambda_2}\right) + \frac{G_8}{c\,\mu}\left(\frac{\partial W}{\partial \lambda_1}\right)\left(\frac{\partial W}{\partial \lambda_3}\right) + \frac{G_9}{c\,\mu}\left(\frac{\partial W}{\partial \lambda_2}\right)\left(\frac{\partial W}{\partial \lambda_3}\right) \end{aligned} \tag{76}$$

where the coefficients $G_0$ through $G_9$ are explicit funtions of the macroscopic stretches $\lambda_1$, $\lambda_2$, $\lambda_3$ given by the expressions in the Appendix. The viscosity solution of the Hamilton-Jacobi equation (75)-(76) cannot be written in closed form. It is possible to complete a variational solution for it (Lopez-Pamies, 2013):

$$\begin{aligned} W^{UB} \;=\; & \frac{3(1-c)}{2(3+2c)}\left[\lambda_1^2 + \lambda_2^2 + \lambda_3^2 - 3\right] \\ & + \frac{3\mu(J-1)}{2J^{1/3}}\left[2 + \frac{1}{J-1} - \frac{(1-c)J^{1/3}(3J^{2/3}+2c)}{(3+2c)(J-1)} - \frac{c^{1/3}J^{1/3}(2J+c-2)}{(J-1)(J-1+c)^{1/3}}\right] \end{aligned} \tag{77}$$

The same PDE can be rewritten in times of the following combination of streches

$$\Lambda_1 = \frac{\lambda_2}{\lambda_1} \qquad \Lambda_2 = \frac{\lambda_3}{\lambda_2} \qquad J = \lambda_1\lambda_2\lambda_3 \tag{78}$$

and is equal to

$$c\frac{\partial \hat{W}}{\partial c} - \hat{W} + \mu\,\hat{G}_0(\Lambda_1,\Lambda_2,J) + \frac{\hat{G}_1(\Lambda_1,\Lambda_2)}{J}\frac{\partial \hat{W}}{\partial \Lambda_1} + \frac{\hat{G}_2(\Lambda_1,\Lambda_2)}{J}\frac{\partial \hat{W}}{\partial \Lambda_2} + \frac{\hat{G}_3(\Lambda_1,\Lambda_2)}{\mu J^{2/3}}\frac{\partial W}{\partial \Lambda_1}\frac{\partial \hat{W}}{\partial \Lambda_2}$$
$$+\frac{\hat{G}_4(\Lambda_1,\Lambda_2)}{\mu J^{2/3}}\Big(\frac{\partial \hat{W}}{\partial \Lambda_1}\Big)^2 + \frac{\hat{G}_5(\Lambda_1,\Lambda_2)}{\mu J^{2/3}}\Big(\frac{\partial \hat{W}}{\partial \Lambda_2}\Big)^2 = 0 \tag{79}$$

with initial condition $W(\Lambda_1,\Lambda_2,J,1) = 0$, all the coefficients of the previous PDE can be found in the Appendix . A last remark to make in this section is that a logarithmic change of variables was also implemented because of stability issues.

### 4.1 Finite element calculations

Finite element calculations are carried out in order to have comparison data for the WENO scheme. By definition, an isotropic distribution of spherical particles involves an infinite number of them. Nonetheless, generating a composite with infinitely many particles (pores) is not computationally feasible. In that sense, we proceed to use a well-established approximate approach and model, use a distribution of monodisperse spherical particles as an infinite media made of a periodic repetition of a unit cell containing a random distribution of a finite number of spherical particles $N$. (see, e.g., Gusev, 1997; Michel et a1., 1999; Segurado and Llorca 2002; Lopez-Pamies et a1., 2013).

### 4.2 Spherical pores with monodisperse size

To generate the monodisperse structure an algorithm is implemented that consists in a sequential addition of particles under certain constrains to the relative distances between pores and to the cell boundary. The radius of each particle is obtained with

$$R_m = L\left(\frac{3c}{4\pi N}\right)^{1/3} \tag{80}$$

In order to not have overlapping between pores and in that way guarantee the volume fraction the following constrains are enforced

- The distance between two different particles, i and j, say where i, j can take values from 1 to $N$, must be greater than a minimum value $s_1$, with an adjustment factor $d_1 = 0.02$.

$$||\mathbf{X}^i - \mathbf{X}^j - \mathbf{h}|| \geq s_1, \quad with \quad s_1 = 2R_m(1+d_1) \tag{81}$$

- The particles have to be at least a minimum distance $s_2$ to the boundaries of the unit cell, making use of an offset factor $d_2 = 0.05$.

$$|X_k^i - R^{(m)}| \geq s_2, \quad |X_k^i + R_m - L| \geq s_2, \quad s_2 = d_2 R_m \qquad (k = 1, 2, 3) \tag{82}$$

for $i = 1, 2, ..., N$. To aid visualization Figure 10 shows the generated microstructures for concentration of pores of five and ten percent. The number of particles was taken as 30, given that by carrying out tests it was found that a number of 30 particles was enough to simulate an isotropic material.

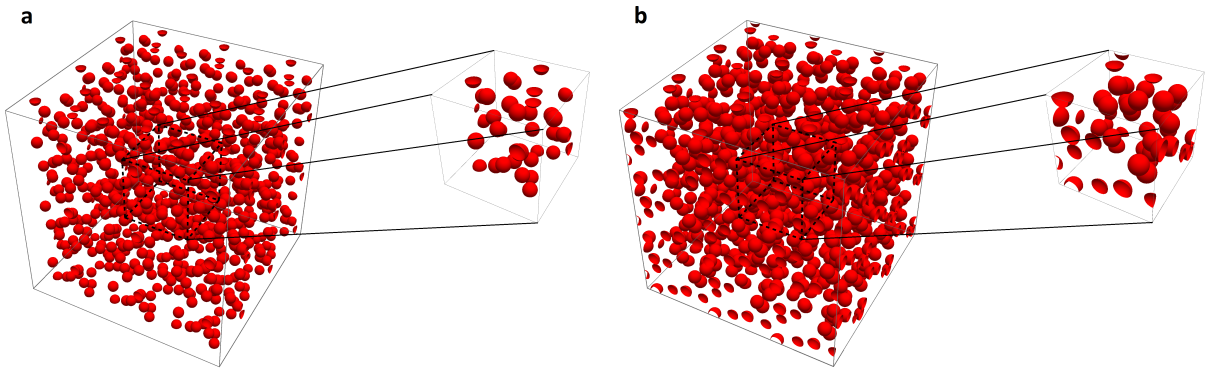


Figure 10: Periodic isotropic porous elastomer model with a representative unit cell $L^3$ containing $N$=30 randomly distributed spherical particles of monodisperse size for the concentrations of (a) $c$=0.05 and (b) $c$=0.10.

### 4.3 Meshing

For the discretization of the monodisperse particles we turn to the mesh generator code Netgen (Shober, 1997), having the ability to produce periodic meshes. For the FEM calculations we make use of a hybrid type of element which can deal with the incompressibility restriction behavior of the matrix a ten node tetrahedral hybrid element. Making use of the FE package ABAQUS, using C3D10H elements (see ABAQUS version 6.13 Documentation). Mesh sensitivity studies reveal that meshes of approximately 60000 elements are enough to produce accurate results. The elastic response of the homogenized material is obtained by enforcing periodic boundary conditions in the unit cell equal to

$$\begin{aligned} u_k(L, X_2, X_3) - u_k(0, X_2, X_3) &= (\overline{F}_{k1} - \delta_{k1})L \\ u_k(X_1, L, X_3) - u_k(X_1, 0, X_3) &= (\overline{F}_{k2} - \delta_{k2})L \\ u_k(X_1, X_2, L) - u_k(X_1, X_2, L) &= (\overline{F}_{k3} - \delta_{k3})L \end{aligned} \tag{83}$$

(k=1,2,3), and computing the total energy $\overline{W}$, using a Cartesian frame reference $\{\mathbf{e}_k\}$ with center at one of the corners of the cube, $\delta_{kl}$ represents the delta de Kronecker symbol, and $\overline{\mathbf{F}}$ is the prescribed

macroscopic deformation gradient. The following figure shows examples of the discretization done with NETGEN.

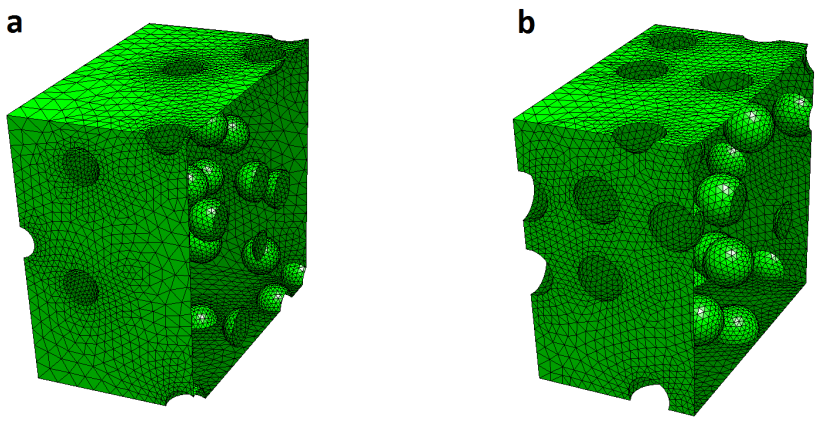


Figure 11: Representative meshes in the reference configuration for monodisperse set of particles (a) $c$=0.05 and (b) $c$=0.10.

### 4.4 Results

By using the finite difference scheme the values of the energy are obtained at discrete points values of the grid. In this way in order to obtain comparison FEM results, the energy is calculated fixing $\Lambda_1, \Lambda_2$ and then varying $J$, as can be seen in Figures 12 and 13, two different plots are shown at each figure in one all the obtained FEM data is shown and in the other the comparison for $\Lambda_2 = 1.00$ is shown. We can remark that for $\Lambda_1 = 1.00$ and $\Lambda_2 = 1.00$ (Hydrostatic loading path) the variational solution is the exact solution of the PDE and therefore is an indicator of the convergence behavior of the scheme, for all other values the variational solution is only an approximation. FEM calculations can only be obtained at relatively small deformations that is why in the plots the domain for $\Lambda_1, \Lambda_2$ are the finite values $\{1.00\ 1.96\ 2.93\ 3.35\}$.

It is important to mention that given that the homogenized material is an isotropic material the elastic energy should be symmetric with respect to the diagonal stretches $\lambda_1$, $\lambda_2$ and $\lambda_3$, in consequence $W(\lambda_1, \lambda_2, \lambda_3) = W(\lambda_2, \lambda_1, \lambda_3) = W(\lambda_1, \lambda_3, \lambda_2) = W(\lambda_2, \lambda_3, \lambda_1) = W(\lambda_3, \lambda_1, \lambda_2) = W(\lambda_3, \lambda_2, \lambda_1)$ these same symmetries can be translated in the variables $\Lambda_1, \Lambda_2, J$ as $\hat{W}(\Lambda_1, \Lambda_2, J) = \hat{W}(\Lambda_1^{-1}, \Lambda_1\Lambda_2, J) = \hat{W}(\Lambda_1\Lambda_2, \Lambda_2^{-1}, J) = \hat{W}(\Lambda_2, \Lambda_1^{-1}\Lambda_2^{-1}, J) = \hat{W}(\Lambda_1^{-1}\Lambda_2^{-1}, \Lambda_1, J) = \hat{W}(\Lambda_1^{-1}, \Lambda_2^{-1}, J)$. Due to that an inverse of each variable is involved in the symmetries and both $\Lambda_1$ and $\Lambda_2$ have to be positive, there is only the need of calculating the regions where $\Lambda_1$ and $\Lambda_2$ are greater than one. The calculations where done with an implicit time integration given its stability and accuracy properties as was shown in section 3, with 2197 grid points.

It can be seen from the results that there is a reasonable agreement between the variational solution, the FEM and WENO scheme calculations. The energy obtained with the WENO scheme seems to have a slightly lower value than the other two methods, for the volume fraction of $c_0 = 0.05$ there is a wider difference between values. As mentioned previously as the concentration reaches

zero the accuracy and convergence rate of the method diminish, more even in this case where the extrapolation is carried out in a larger number of points.

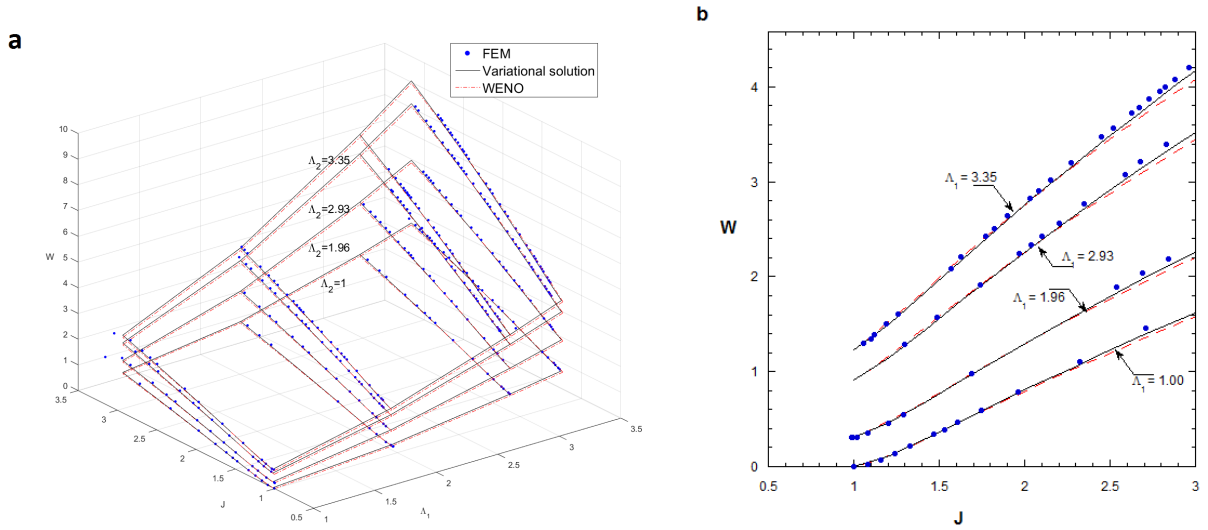


Figure 12: Comparison of the different methods for the macroscopic energy of a neo-hookean matrix weakened by pores under diagonal loading. (a) Comparison for different constant values of $\Lambda_1$, $\Lambda_2$. (b) Level curves for $\Lambda_2 = 1.00$. Volume fraction of $c_0 = 0.10$

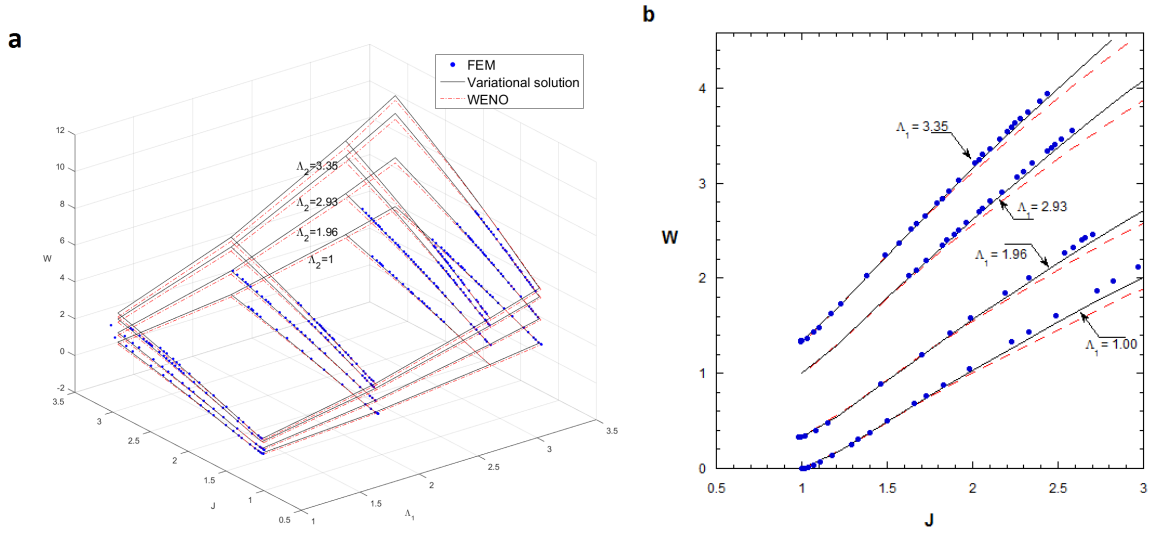


Figure 13: Comparison of the different methods for the macroscopic energy of a neo-hookean matrix weakened by pores under diagonal loading. (a) Comparison for different constant values of $\Lambda_1$, $\Lambda_2$. (b) Level curves for $\Lambda_2 = 1.00$. Volume fraction of $c_0 = 0.05$

# 5 Conclusions

Several marching methods have been proposed in the literature for solving conservations laws and time dependent Hamilton-Jacobi equations. Nevertheless, we remark that the equations solved until now where linear equations or/and periodic boundary conditions where enforced.

For this reason and given that we are interested in solving H-J equations of the form (1)-(2) a WENO scheme is developed. In order to assess the convergence, accuracy and stability of the scheme this same one was tested for equations of the form (1)-(2) with specific deformation gradients and Lagrangian electric fields. A one space variable hydrostatic loading path and a two space variable planar deformation path. Just by implementing the scheme in the original set of coordinates it was found instable and a logarithmic change of variable that stretches time and space was needed. After having carried out all the calculation and once obtained the convergence rates it was observed that the method is not alwasys fifth order and as the time integration increases the convergence rate keeps diminishing. All the previous evidence seems to suggest that the cause are the numerical boundary conditions, hypothesis that is furthermore enforced in section 3.4, where by using a fifty percent of the whole domain the convergence rates where always fifth order until very low concentrations, indicating that by taking points closer to the boundary the convergence diminishes.

Once the convergence of the finite difference scheme was proved, we make use of the method to obtain a solution of a problem for which there is not a close solution an equation of the type (1)-(2) under a diagonal deformation displacement gradient (73). FEM calculation were carried out to have comparison data, then by comparing the FDM, FEM and variational solution calculations, we can see that there is quite good agreement between them. With the FEM calculations exhibiting a slightly stiffer behavior than the variational solution and the WENO scheme a softer behavior.

One of the most important contribution of this work is the presentation of proofs of the phenomena; that the convergence and stability of the marching method used to solve time dependent Hamilton-Jacobi equations (ENO  WENO schemes) depends on the boundary conditions, a practical extension of this work would consists in further investigate the issues of the boundary conditions to have a method of fifth order convergence for any "time".

## References


[1] Bardi, M. and Capuzzo-Dolcetta, I., 2008. *Optimal control and viscosity solutions of Hamilton-Jacobi-Bellman equations*. Springer Science & Business Media.

[2] Benton, S.H., 1977. *The Hamilton-Jacobi equation*. Elsevier.

[3] Butcher, J.C., 1987. *The numerical analysis of ordinary differential equations: Runge-Kutta and general linear methods*. Wiley-Interscience.

[4] Bryson, S. and Levy, D., 2003. *High-order semi-discrete central-upwind schemes for multi-dimensional Hamilton-Jacobi equations. Journal of Computational Physics*, 189(1), pp.63-87.

[5] Crandall, M.G. and Lions, P.L., 1983. *Viscosity solutions of Hamilton-Jacobi equations. Transactions of the American Mathematical Society*, 277(1), pp.1-42.

[6] Crandall, M.G. and Lions, P.L., 1984. *Two approximations of solutions of Hamilton-Jacobi equations. Mathematics of Computation*, 43(167), pp.1-19.

[7] Evans, L.C., 2010. *Partial Differential Equations*. The American Mathematical Society.

[8] Gottlieb, S., Shu, C.W. and Tadmor, E., 2001. *Strong stability-preserving high-order time discretization methods*. SIAM review, 43(1), pp.89-112.

[9] Henrick, A.K., Aslam, T.D. and Powers, J.M., 2005. *Mapped weighted essentially non-oscillatory schemes: achieving optimal order near critical points. Journal of Computational Physics*, 207(2), pp. 542-567.

[10] Jiang, G.S. and Shu, C.W., 1995. *Efficient implementation of weighted ENO schemes. J. Comput. Phys. 126, 202-228.*

[11] Jiang, G.S. and Peng, D., 2000. *Weighted ENO schemes for Hamilton–Jacobi equations. SIAM Journal on Scientific computing*, 21(6), pp.2126-2143.

[12] Kurganov, A., Noelle, S. and Petrova, G., 2001. *Semidiscrete central-upwind schemes for hyperbolic conservation laws and Hamilton–Jacobi equations. SIAM Journal on Scientific Computing*, 23(3), pp.707-740.

[13] Lawson, J.D., 1966. *An order five Runge-Kutta process with extended region of stability. SIAM Journal on Numerical Analysis*, 3(4), pp.593-597.

[14] Liu, X.D., Osher, S. and Chan, T., 1994. *Weighted essentially non-oscillatory schemes. Journal of computational physics*, 115(1), pp.200-212.

[15] Lopez-Pamies, O., 2006. *On the effective behavior, microstructure evolution, and macroscopic stability of elastomeric composites*, Ph.D. Dissertation University of Pennsylvania, USA.

[16] Lopez-Pamies, O., 2013. Unpublished work.

[17] Lopez-Pamies, O., 2014. *Elastic dielectric composites: Theory and application to particle-filled ideal dielectrics. Journal of the Mechanics and Physics of Solids*, 64, pp.61-82.

[18] Lopez-Pamies, O. and Idiart, M.I., 2009. *An exact result for the macroscopic response of porous Neo-Hookean solids. Journal of Elasticity*, 95(1-2), pp.99-105.

[19] Lopez-Pamies, O., Idiart, M.I. and Nakamura, T., 2011. *Cavitation in elastomeric solids: I A defect-growth theory. Journal of the Mechanics and Physics of Solids*, 59(8), pp.1464-1487.

[20] Lopez-Pamies, O., Nakamura, T. and Idiart, M.I., 2011. *Cavitation in elastomeric solids: II Onset-of-cavitation surfaces for Neo-Hookean materials. Journal of the Mechanics and Physics of Solids*, 59(8), pp.1488-1505.

[21] Lopez-Pamies, O., Goudarzi, T. and Nakamura, T., 2013. *The nonlinear elastic response of suspensions of rigid inclusions in rubber: I an exact result for dilute suspensions. Journal of the Mechanics and Physics of Solids*, 61(1), pp.1-18.

[22] Osher, S. and Sethian, J.A., 1988. *Fronts propagating with curvature-dependent speed: algorithms based on Hamilton-Jacobi formulations. Journal of computational physics*, 79(1), pp.12-49.

[23] Osher, S. and Shu, C.W., 1991. *High-order essentially nonoscillatory schemes for Hamilton-Jacobi equations. SIAM Journal on numerical analysis*, 28(4), pp.907-922.

[24] Osher, S. and Fedkiw, R., 2006. *Level set methods and dynamic implicit surfaces (Vol. 153). Springer Science & Business Media.*

[25] Shu, C.W., 2009. *High order weighted essentially nonoscillatory schemes for convection dominated problems. SIAM review*, 51(1), pp.82-126.

[26] Shu, C.W. and Osher, S., 1988. *Efficient implementation of essentially non-oscillatory shock-capturing schemes. Journal of Computational Physics*, 77(2), pp.439-471.

[27] Tan, S. and Shu, C.W., 2010. *Inverse Lax-Wendroff procedure for numerical boundary conditions of conservation laws. Journal of Computational Physics*, 229(21), pp.8144-8166.

[28] Toro, E.F., 2013. *Riemann solvers and numerical methods for fluid dynamics: a practical introduction.* Springer Science & Business Media.

[29] Xing, Y. and Shu, C.W., 2011. *High-order finite volume WENO schemes for the shallow water equations with dry states.* Advances in Water Resources, 34(8), pp.1026-1038.

## Appendix A. Coefficients $G_i$ and $\hat{G}_i$ in Hamiltonians (76) and (79)

$$
\begin{aligned}
G_0 =& \frac{1}{3}(\lambda_1^2+\lambda_2^2+\lambda_3^2) - \frac{3}{2} + \frac{\Gamma_F}{2\lambda_1\lambda_2\lambda_3^2} \\
G_1 =& \frac{\Gamma_E\lambda_1(\lambda_3^2-\lambda_3^3)}{\lambda_3(\lambda_1^2-\lambda_2^2)(\lambda_1^2-\lambda_3^2)} + \frac{\Gamma_F\lambda_1}{\lambda_1^2\lambda_3-\lambda_3^3} + \frac{\lambda_2}{\lambda_1^2\lambda_3-\lambda_2^2\lambda_3} + \frac{\lambda_1}{3} \\
G_2 =& \frac{\lambda_2}{3} - \frac{\lambda_1-\Gamma_E\lambda_2}{\lambda_1^2\lambda_3-\lambda_2^2\lambda_3} \\
G_3 =& \frac{3(\Gamma_F-\Gamma_E)+\lambda_1^2\lambda_3-\lambda_3^3}{3(\lambda_1^2-\lambda_3^2)} \\
G_4 =& \frac{\lambda_1^2(\lambda_1^4-\lambda_3^2(\lambda_1^2+\lambda_2^2)+2\lambda_1^2\lambda_2^2-\lambda_2^4)}{6(\lambda_1^2-\lambda_2^2)^2\,(\lambda_1^2-\lambda_3^2)} + \frac{\Gamma_E\lambda_1^3\lambda_2(\lambda_2^2-\lambda_3^2)(-2\lambda_1^2+\lambda_2^2+\lambda_3^2)}{3(\lambda_1^2-\lambda_2^2)^2\,(\lambda_1^2-\lambda_3^2)^2} \\
& \frac{\Gamma_F\lambda_1^3\lambda_2(-3\lambda_1^2+2\lambda_2^2+\lambda_3^2)}{6(\lambda_1^2-\lambda_2^2)\,(\lambda_1^2-\lambda_3^2)^2} \\
G_5 =& \frac{\lambda_2^2(-2\Gamma_E\lambda_1\lambda_2(\lambda_1^2-2\lambda_2^2+\lambda_3^2)+\Gamma_F\lambda_1\lambda_2(\lambda_1^2-\lambda_2^2)+\lambda_1^4+\lambda_3^2(\lambda_1^2+\lambda_2^2)-2\lambda_1^2\lambda_2^2-\lambda_2^4)}{6(\lambda_1^2-\lambda_2^2)^2\,(\lambda_2^2-\lambda_3^2)} \\
G_6 =& -\frac{\lambda_3^2(-2\Gamma_E\lambda_1\lambda_2(\lambda_1^2+\lambda_2^2-2\lambda_3^2))+\Gamma_F\lambda_1\lambda_2(\lambda_1^2+2\lambda_2^2-3\lambda_3^2)+(\lambda_1^2-\lambda_3^2)(\lambda_1^2+\lambda_2^2-\lambda_3^2)}{6(\lambda_1^2-\lambda_2^2)^2\,(\lambda_2^2-\lambda_3^2)} \\
G_7 =& \frac{\lambda_1\lambda_2(-\Gamma_E\lambda_1\lambda_2(\lambda_1^2+\lambda_2^2-2\lambda_3^2)+\Gamma_F\lambda_1\lambda_2(\lambda_2^2-\lambda_1^2)+(\lambda_1^2+\lambda_2^2)(\lambda_1^2-\lambda_3^2))}{3(\lambda_1^2-\lambda_2^2)^2\,(\lambda_1^2+\lambda_2^2)^2\,(\lambda_1^2-\lambda_3^2)} \\
G_8 =& \frac{\lambda_1\lambda_2\lambda_3(\Gamma_E\lambda_1(\lambda_1^2-2\lambda_2^2+\lambda_3^2)+2\Gamma_F\lambda_1(\lambda_2^2-\lambda_1^2)+\lambda_2^2(\lambda_1^2-\lambda_3^2))}{3(\lambda_1^2-\lambda_2^2)(\lambda_1^2-\lambda_3^2)^2} \\
G_9 =& -\frac{\lambda_1\lambda_2\lambda_3(\Gamma_E\lambda_2(-2\lambda_1^2+\lambda_2^2+\lambda_3^2)+2\Gamma_F\lambda_2(\lambda_1^2-\lambda_2^2)+\lambda_1(\lambda_1^2-\lambda_3^2))}{3(\lambda_1^2-\lambda_2^2)\,(\lambda_1^2-\lambda_3^2)\,(\lambda_1^2-\lambda_3^2)}
\end{aligned}
\tag{84}
$$

In the above coefficients

$$
\Gamma_F = \frac{\lambda_3}{\sqrt{\lambda_3^2-\lambda_2^2}}\,\varepsilon_F\left\{\frac{\sqrt{\lambda_3^2-\lambda_2^2}}{2\sqrt{\lambda_2^2-\lambda_3^2}}\ln\left[\frac{2\lambda_2(\lambda_2+\sqrt{\lambda_2^2-\lambda_3^2}}{\lambda_3^2}-\right]\;;\;\frac{\lambda_1^2-\lambda_3^2}{\lambda_2^2-\lambda_3^2}\right\} \tag{85}
$$

$$
\Gamma_E = \frac{\lambda_3}{\sqrt{\lambda_3^2-\lambda_2^2}}\,\varepsilon_E\left\{\frac{\sqrt{\lambda_3^2-\lambda_2^2}}{2\sqrt{\lambda_2^2-\lambda_3^2}}\ln\left[\frac{2\lambda_2(\lambda_2+\sqrt{\lambda_2^2-\lambda_3^2}}{\lambda_3^2}-\right]\;;\;\frac{\lambda_1^2-\lambda_3^2}{\lambda_2^2-\lambda_3^2}\right\} \tag{86}
$$

The coefficients for the PDE in times of its variables $(\Lambda_1, \Lambda_2, J)$

$$
\begin{aligned}
\hat{G}_0 =& -\frac{3}{2} + \frac{J^{2/3}[(\Lambda_1^2+1)\Lambda_2^2+1]}{3\Lambda_1^{2/3}\Lambda_2^{4/3}} + \frac{\Lambda_1^{1/3}\Lambda_2^{2/3}}{2J^{4/3}}\,\hat{\Gamma}_F \\
\hat{G}_1 =& \frac{\Lambda_1^3+\Lambda_1}{\Lambda_1^2-1} - \frac{\Lambda_1^2[(\Lambda_1^2+1)\Lambda_2^2-2]}{(\Lambda_1^2-1)(\Lambda_1^2\Lambda_2^2-1)}\,\hat{\Gamma}_E + \frac{\Lambda_1^2\Lambda_2^2}{1-\Lambda_1^2\Lambda_2^2}\,\hat{\Gamma}_F \\
\hat{G}_2 =& \frac{\Lambda_1^2\Lambda_2}{\Lambda_1^2-1} + \frac{\Lambda_1\Lambda_2[(2\Lambda_1^2-1)\Lambda_2^2-1]}{(\Lambda_1^2-1)(\Lambda_1^2\Lambda_2^2-1)}\,\hat{\Gamma}_E + \frac{\Lambda_1\Lambda_2^3}{1-\Lambda_1^2\Lambda_2^2}\hat{\Gamma}_F \\
\hat{G}_3 =& \frac{\Lambda_1^{5/3}\Lambda_2^{1/3}[-(5\Lambda_1^2+3)\Lambda_2^2+2(\Lambda_1^2+1)+(-2\Lambda_1^6+4\Lambda_1^4+\Lambda_1^2+1)\Lambda_2^2]}{3(\Lambda_1^2-1)^2(\Lambda_2^2-1)(\Lambda_1^2\Lambda_2^2-1)} \\
& -\frac{\Lambda_1^{8/3}\Lambda_2^{1/3}[(\Lambda_1^2-2)\Lambda_2^2+1][\Lambda_2^2(4\Lambda_1^4\Lambda_2^2-\Lambda_1^2(\Lambda_2^2+7)+\Lambda_2^2-1)+4]}{3(\Lambda_1^2-1)^2(1-\Lambda_2^2)(\Lambda_1^2\Lambda_2^2-1)^2}\,\hat{\Gamma}_E \\
& \frac{2\Lambda_1^{8/3}\Lambda_2^{7/3}[-(\Lambda_1^2+1)\Lambda_2^2+(\Lambda_1^4-\Lambda_1^2+1)\Lambda_2^4+1]}{3(\Lambda_1^2-1)^2(1-\Lambda_2^2)(\Lambda_1^2\Lambda_2^2-1)^2}\,\hat{\Gamma}_F \\
\hat{G}_4 =& \frac{\Lambda_1^{8/3}[(\Lambda_1^2+3)(3\Lambda_1^2+1)\Lambda_2^2-4(\Lambda_1^2+1)+(\Lambda_1^6-5\Lambda_1^4-5\Lambda_1^2+1)\Lambda_2^4]}{6(\Lambda_1^2-1)^2\Lambda_2^{2/3}(\Lambda_2^2-1)(\Lambda_1^2\Lambda_2^2-1)} \\
& +\frac{\Lambda_1^{11/3}[12\Lambda_1^2\Lambda_2^4-6(\Lambda_1^2+1)\Lambda_2^2+(\Lambda_1^2+1)(\Lambda_1^4-4\Lambda_1^2+1)\Lambda_2^6+4]}{3(\Lambda_1^2-1)^2\Lambda_2^{2/3}(1-\Lambda_2^2)(\Lambda_1^2\Lambda_2^2-1)^2}\hat{\Gamma}_E \\
& -\frac{\Lambda_1^{11/3}\Lambda_2^{4/3}[-(7\Lambda_1^2+1)\Lambda_2^2+(\Lambda_1^4+5\Lambda_1^2-2)\Lambda_2^4+4]}{6(\Lambda_1^2-1)(1-\Lambda_2^2)(\Lambda_1^2\Lambda_2^2-1)^2}\,\hat{\Gamma}_F \\
\hat{G}_5 =& \frac{\Lambda_1^{2/3}\Lambda_2^{4/3}[\Lambda_1^2(7-3\Lambda_1^2)\Lambda_2^2-\Lambda_1^2+(4\Lambda_1^6-5\Lambda_1^4-2\Lambda_1^2+1)]\Lambda_2^4-1)}{6(\Lambda_1^2-1)^2(\Lambda_2^2-1)(\Lambda_1^2\Lambda_2^2-1)} \\
& +\frac{\Lambda_1^{5/3}\Lambda_2^{4/3}((4\Lambda_1^6-6\Lambda_1^4+1)\Lambda_2^6-3(2\Lambda_1^4-4\Lambda_1^2+1)\Lambda_2^4-3\Lambda_2^2+1)}{3(\Lambda_1^2-1)^2(1-\Lambda_2^2)(\Lambda_1^2\Lambda_2^2-1)^2}\,\hat{\Gamma}_E \\
& -\frac{\Lambda_1^{5/3}\Lambda_2^{10/3}[(5-7\Lambda_1^2)\Lambda_2^2+(4\Lambda_1^4-\Lambda_1^2-2)\Lambda_2^4+1]}{6(\Lambda_1^2-1)(1-\Lambda_2^2)(\Lambda_1^2\Lambda_2^2-1)^2}\,\hat{\Gamma}_F
\end{aligned}
\tag{87}
$$

with

$$
\hat{\Gamma}_F = \frac{1}{\sqrt{1-\Lambda_2^2}}\,\varepsilon_F\left\{\frac{\sqrt{1-\Lambda_2^2}}{2\sqrt{\Lambda_2^2-1}}\ln[2\Lambda_2(\Lambda_2+\sqrt{\Lambda_2^2-1})-1\,;\ \frac{\Lambda_1^2\Lambda_2^2-1}{\Lambda_2^2-1}\right\} \tag{88}
$$

$$
\hat{\Gamma}_E = \frac{1}{\sqrt{1-\Lambda_2^2}}\,\varepsilon_E\left\{\frac{\sqrt{1-\Lambda_2^2}}{2\sqrt{\Lambda_2^2-1}}\ln[2\Lambda_2(\Lambda_2+\sqrt{\Lambda_2^2-1})-1\,;\ \frac{\Lambda_1^2\Lambda_2^2-1}{\Lambda_2^2-1}\right\} \tag{89}
$$

## Appendix B. Hamilton-Jacobi equations and marching methods

This appendix presents an introduction of Hamilton-Jacobi equations and respective marching methods to solve them. Time dependent Hamilton-Jacobi equations of the form of (90) almost never have classical solutions that is why there is a need of introducing generalized solutions

$$\begin{cases} \partial u/\partial t + H(Du, u, x, t) = 0 & \text{in } \mathbf{R}^N \times (0, \infty) \\ u(x, 0) = u_0(x) & \text{in } \mathbf{R}^N \end{cases} \tag{90}$$

A uniquely generalized solution for this class of equations are the so called viscosity solutions. These kind of solutions are of primary interest in many areas of application (optimization, control theory, differential games, etc). The name viscosity solution comes from the fact that they can be obtained via the method of vanishing viscosity. The method of vanishing viscosity consists in solving problem

$$\begin{cases} \partial u^\epsilon/\partial t + H(Du^\epsilon, u^\epsilon, x, t) - \epsilon\, \Delta u^\epsilon = 0 & \text{in } \mathbf{R}^N \times (0, \infty) \\ u(x, 0) = u_0(x) & \text{in } \mathbf{R}^N \end{cases} \tag{91}$$

with u being the viscosity solution of the original problem, one can show that $|u^\epsilon(x,t) - u(x,t)| \leq c\sqrt{\epsilon}$ for x $\in \mathbf{R}^N$ and $t > 0$. Thus by taking $\epsilon \to 0$ one can obtain the viscosity solution of the original problem.

In order to solve equation (90) the marching method first proposed by Crandall and Lions (1983) is

$$U^{n+1}_{j,k} = G(x_j, y_k, t_n, U^n_{j-p,k-r}, ..., U^n_{j+q+1,k+s+1}) \tag{92}$$

in a more simplified notation

$$U^{n+1} = G(U^n) \tag{93}$$

where p, q, r, s are fixed positive integers and G is a function of (p+q+2)(r+s+2) variables. Most of the literature of these kind of methods (ENO-WENO schemes) use explicit integration in time, however in this report we also explore the possibility of using implicit integration because of their numerical stability. A point in $R^2$ will have coordinates (x,y), where $Du = (u_x, u_y)$. The mesh sizes $\Delta x, \Delta y, \Delta t > 0$, $U^n_{j,k}$ is the numerical approximation at $(x_j, y_k, t_n) = (j\Delta x, k\Delta y, n\Delta t)(j, k, n) \in \mathbf{Z}$, $U^n$ is the numerical approximation at time $n\Delta t$. The notation for the difference $\Delta^x_+ = U^n_{j+1,k} - U^n_{j,k}$, and $\Delta^y_+ = U^n_{j,k+1} - U^n_{j,k}$, is used. We say that equation (92) has differenced form if there is a function $\hat{H}$ called the numerical Hamiltonian such that

$$G(x_j, y_k, t_n, U^n_{j-p,k-r}, ..., U^n_{j+q+1,k+s+1}) = U^n_{j,k} - \Delta t \hat{H}\Big(x_j, y_k, t_n, \frac{\Delta^x_+}{\Delta x} U^n_{j-p,k-r}, ..., \frac{\Delta^x_+}{\Delta x} U^n_{j+q+1,k+s+1}, \frac{\Delta^y_+}{\Delta y} U^n_{j-p,k-r}, ..., \frac{\Delta^y_+}{\Delta y} U^n_{j+q+1,k+s+1}\Big) \tag{94}$$

where $\hat{H}$ has to be consistent with $u_t + H(u_x, u_y) = 0$, i.e.

$$\hat{H}(x_i, y_j, t_n, a, ..., a; b, ..., b) = H(x_i, y_j, t_n, a, b) \quad \text{for} \in \mathbf{R} \tag{95}$$

The numerical Hamiltonian is monotone on [-R, R] if $G(U^n_{j-p,k-r}, ..., U^n_{j+q+1,k+s+1})$ is non-decreasing function of each argument as long as each difference $|\Delta^x_+ U_{l,m}|$, $|\Delta^y_+ U_{l',m'}| \leq R$ for $j - p \leq l \leq j + q + 1$, $k - r \leq m \leq k + s + 1$, $j - p \leq l' \leq j + q + 1$, $k - r \leq m' \leq k + s$. In other words R will be an a priori bound of $|u_x|$, $|u_y|$. The convergence for this numerical approximations to the viscosity solution was proven in [6] and relies on the following theorem

**Theorem 1**

Let H: $\mathbf{R}^2 \to \mathbf{R}$ be continuous and $u_0$ be Lipschitz continuous on $\mathbf{R}^2$ with L as a Libschitz constant. For $\Delta t/\Delta x, \Delta t/\Delta y > 0$ and fixed, let the scheme (92) have differenced form, be monotone on $[-(L+1), L+1]$ and be consistent with (90). Assume the numerical Hamiltonian g is locally Lipschitz continuous. Define $U^0$ by $U^0_{j,k} = u_0(x_j, y_k)$ and then $U^n$, n=1,2,... by (92). Let u be the viscosity solution of (90). Then there is a constant $\mathcal{K}$ depending only on $sup|u_0|$, L, g and N$\Delta t$ such that

$$|U^n_{j,k} - u(x_j, y_k, n\Delta t)| \leq \mathcal{K}\sqrt{\Delta t} \tag{96}$$

for $0 \leq n \leq M$ and all j, k.

In the literature Osher and Sethian (1988) where the first to introduce these kind of methods for specific problems, another works in the same area are the ones of Jiang and Peng (2000) and Bryson and Levy (2003).